5

Conserving Integrators for Parallel Manipulators

Stefan Uhlar and Peter Betsch
Chair of Computational Mechanics, Department of Mechanical Engineering, University of Siegen
Germany

1. Introduction

The present work deals with the development of time stepping schemes for the dynamics of parallel manipulators. In particular, we aim at energy and momentum conserving algorithms for a robust time integration of the differential algebraic equations (DAEs) which govern the motion of closed-loop multibody systems. It is shown that a rotationless formulation of multibody dynamics is especially well-suited for the design of energy-momentum schemes. Joint coordinates and associated forces can still be used by applying a specific augmentation technique which retains the advantageous algorithmic conservation properties. It is further shown that the motion of a manipulator can be partially controlled by appending additional servo constraints to the DAEs.

Starting with the pioneering works by Simo and co-workers [SW91, STW92, ST92], energy-momentum conserving schemes and energy-decaying variants thereof have been developed primarily in the context of nonlinear finite element methods. In this connection, representative works are due to Brank et al. [BBTD98], Bauchau & Bottasso [BB99], Crisfield & Jelenić [CJ00], Ibrahimbegović et al. [IMTC00], Romero & Armero [RA02], Betsch & Steinmann [BS01a], Puso [Pus02], Laursen & Love [LL02] and Armero [Arm06], see also the references cited in these works.

Problems of nonlinear elastodynamics and nonlinear structural dynamics can be characterized as stiff systems possessing high frequency contents. In the conservative case, the corresponding semi-discrete systems can be classified as finite-dimensional Hamiltonian systems with symmetry. The time integration of the associated nonlinear ODEs by means of energy-momentum schemes has several advantages. In addition to their appealing algorithmic conservation properties energy-momentum schemes are known to possess enhanced numerical stability properties (see Gonzalez & Simo [GS96]). Due to these advantageous properties energy-momentum schemes have even been successfully applied to penalty formulations of multibody dynamics, see Goicolea & Garcia Orden [GGO00]. Indeed, the enforcement of holonomic constraints by means of penalty methods again yields stiff systems possessing high frequency contents. The associated equations of motion are characterized by ODEs containing strong constraining forces. In the limit of infinitely large penalty parameters these ODEs replicate Lagrange's equations of motion of the first kind (see Rubin & Ungar [RU57]), which can be identified as index-3 differential-algebraic equations (DAEs). This observation strongly supports the expectation that energy-

Source: Parallel Manipulators, New Developments, Book edited by: Jee-Hwan Ryu, ISBN 978-3-902613-20-2, pp. 498, April 2008, I-Tech Education and Publishing, Vienna, Austria

momentum methods are also beneficial to the discretization of index-3 DAEs (see G´eradin & Cardona [GC01, Chapter 12] and Leyendecker et al. [LBS04]).

The specific formulation of the equations of motion strongly affects the subsequent time discretization. In the context of multibody systems the main distinguishing feature of alternative formulations is the choice of coordinates for the description of the orientation of the individual rigid bodies. For this purpose some kind of rotational variables (e.g. joint-angles, Euler angles or other 3-parameter representations of finite rotations) are often employed. In general, the equations of motion in terms of rotational variables are quite cumbersome. In the case of systems with tree structure one is typically confronted with highly-nonlinear ODEs. Further challenges arise in the case of closed-loop systems due to the presence of algebraic loop-closure constraints leading to index-3 DAEs. As a consequence of their inherent complexity, the design of energy-momentum conserving schemes is hardly conceivable for formulations of general multibody systems involving rotations.

In the present work the use of rotational variables is completely circumvented in the formulation of the equations of motion. Our formulation turns out to be especially well-suited for the energy-momentum conserving integration of both open-loop and closed-loop multibody systems. In our approach the orientation of each rigid body is characterized by the elements of the rotation matrix (or the direction cosine matrix). This leads to a set of redundant coordinates which are subject to holonomic constraints. In this connection two types of constraints may be distinguished (see also Betsch & Steinmann [BS02b]): (i) Internal constraints which are intimately connected to the assumption of rigidity and, (ii) external constraints due to the interconnection of the bodies constituting the multibody system. Item (ii) implies that loop-closure constraints can be taken into account without any additional difficulty. The resulting DAEs exhibit a comparatively simple structure which makes possible the design of energy-momentum conserving schemes. Another advantage of the present rotationless formulation of multibody systems lies in the fact that planar motions as well as spatial motions can be treated without any conceptual differences. That is, the extension from the planar case to the full three-dimensional case can be accomplished in a straightforward way, which is in severe contrast to formulations employing rotations, due to their non-commutative nature in the three-dimensional setting. It is worth mentioning that the present rotationless approach resembles to some degree the natural coordinates formulation advocated by Garcia de Jalon et al. [JUA86].

As pointed out above the rotationless formulation of multibody systems benefits the design of energy-momentum schemes. On the other hand, the advantages for the discretization come at the expense of a comparatively large number of unknowns. In addition to that, joint-angles and associated torques are often required in practical applications, for example, if a joint is actuated. The size of the algebraic system to be solved can be systematically reduced by applying the discrete null space method developed in [Bet05a]. Indeed, the present treatment of planar multibody dynamics fits into the framework proposed in [BL06,LBS]. The main new contributions presented herein are (i) a coordinate augmentation technique which facilitates to incorporate rotational degrees of freedom along with associated torques and, (ii) the incorporation of control constraints in order to perform a controled movement of fully and underactuated multibody systems.

An outline of the rest of the paper is as follows: In Section 2 the formulation of constrained mechanical systems is outlined and the energy-momentum conserving discretization is

introduced. Section 3 contains the advocated description of rigid bodies in terms of redundant coordinates. Section 4 deals with two basic kinematic pairs, i.e. the revolute and prismatic pair as building blocks of multibody systems. In addition to that, the newlyproposed coordinate augmentation technique for the incorporation of joint coordinates and associated torques or forces is presented. The application of the above mentioned features will be carried out with the example of a planar parallel manipulator of RPR type (Section 5). Conclusions are drawn in Section 6.

2. Dynamics of constrained mechanical systems

In the present work we focus on discrete mechanical systems subject to constraints which are holonomic and scleronomic. Due to the specific formulation of rigid bodies (see Section 3) the equations of motion for multibody systems can be written in the form

$$\begin{aligned} \dot{\boldsymbol{q}} - \boldsymbol{v} &= \boldsymbol{0} \\ \boldsymbol{M}\dot{\boldsymbol{v}} - \boldsymbol{F} + \boldsymbol{G}^T\boldsymbol{\lambda} &= \boldsymbol{0} \\ \boldsymbol{\Phi}(\boldsymbol{q}) &= \boldsymbol{0} \end{aligned} \tag{1}$$

where $\mathbf{q}(t) \in \mathbb{R}^n$ specifies the configuration of the mechanical system at time t, and $\mathbf{v}(t) \in \mathbb{R}^n$ is the velocity vector. Together ($\mathbf{q}$, $\mathbf{v}$) form the vector of state space coordinates (see, for example, Rosenberg [Ros77]). A superposed dot denotes differentiation with respect to time and $\mathbf{M} \in \mathbb{R}^{n\times n}$ is a *constant* and symmetric mass matrix, so that the kinetic energy can be written as

$$T(\boldsymbol{v}) = \frac{1}{2}\boldsymbol{v}\cdot\boldsymbol{M}\boldsymbol{v} \tag{2}$$

Moreover, $\mathbf{F} \in \mathbb{R}^n$ is a load vector which in the present work is decomposed according to

$$\boldsymbol{F} = \boldsymbol{Q} - \nabla V(\boldsymbol{q}) \tag{3}$$

Here, $V(\mathbf{q}) \in \mathbb{R}$ is a potential energy function and $\mathbf{Q} \in \mathbb{R}^n$ accounts for loads which can not be derived from a potential. Moreover, $\boldsymbol{\phi}(\mathbf{q}) \in \mathbb{R}^m$ is a vector of geometric constraint functions, $\mathbf{G} = D\,\boldsymbol{\phi}(\mathbf{q}) \in \mathbb{R}^{m\times n}$ is the constraint Jacobian and $\boldsymbol{\lambda} \in \mathbb{R}^m$ is a vector of multipliers which specify the relative magnitude of the constraint forces. In the above description it is tacitly assumed that the *m* constraints are independent.
Due to the presence of holonomic (or geometric) constraints $(1)_3$, the configuration space of the system is given by

$$\mathsf{Q} = \{\boldsymbol{q}(t) \in \mathbb{R}^n \,|\, \boldsymbol{\Phi}(\boldsymbol{q}) = \boldsymbol{0}\} \tag{4}$$

The equations of motion (1) form a set of index-3 differential-algebraic equations (DAEs) (see, for example, Kunkel & Mehrmann [KM06]). They can be directly derived from the classical Lagrange's equations.

2.1 Energy-momentum discretization

'Experience indicates that the best results can generally be obtained using a direct discretization of the equations of motion.' Leimkuhler & Reich [LR04, Sec. 7.2.1]

2.1.1 The basic energy-momentum scheme

For the direct discretization of the DAEs (1), we employ the methodology developed by Gonzalez [Gon99]. Consider a representative time interval $[t_n,\ t_{n+1}]$ with time step $\Delta t = t_{n+1} - t_n$, and given state space coordinates $\mathbf{q}_n \in Q$, $v_n \in \mathbb{R}^n$ at t_n. The discretized version of (1) is given by

$$\begin{aligned} \boldsymbol{q}_{n+1} - \boldsymbol{q}_n &= \frac{\Delta t}{2}(\boldsymbol{v}_n + \boldsymbol{v}_{n+1}) \\ \boldsymbol{M}(\boldsymbol{v}_{n+1} - \boldsymbol{v}_n) &= \Delta t \mathbf{F}(\boldsymbol{q}_n, \boldsymbol{q}_{n+1}) - \Delta t \mathbf{G}(\boldsymbol{q}_n, \boldsymbol{q}_{n+1})^T \bar{\boldsymbol{\lambda}} \\ \boldsymbol{\Phi}(\boldsymbol{q}_{n+1}) &= \mathbf{0} \end{aligned} \tag{5}$$

with

$$\mathbf{F}(\boldsymbol{q}_n, \boldsymbol{q}_{n+1}) = \mathbf{Q}(\boldsymbol{q}_n, \boldsymbol{q}_{n+1}) - \bar{\nabla} V(\boldsymbol{q}_n, \boldsymbol{q}_{n+1}) \tag{6}$$

In the sequel, the algorithm (5) will be called the basic energy-momentum (***BEM***) scheme. The advantageous algorithmic conservation properties (see Remark 2.1 below) of the BEM scheme are linked to the notion of a discrete gradient (or derivative) of a function $f: \mathbb{R}^n \to \mathbb{R}$. In the present work $\bar{\nabla} f(\mathbf{q}_n,\ \mathbf{q}_{n+1})$ denotes the discrete gradient of f. It is worth mentioning that if f is at most quadratic then the discrete gradient coincides with the standard gradient evaluated in the mid-point configuration $\mathbf{q}_{n+1/2} = (\mathbf{q}_n + \mathbf{q}_{n+1})/2$, that is, in this case $\bar{\nabla} f(\mathbf{q}_n,\ \mathbf{q}_{n+1}) = \nabla f(\mathbf{q}_{n+1/2})$. In $(5)_2$ the discrete gradient is applied to the potential energy function V as well as to the constraint functions ϕ_i. In particular, the discrete constraint Jacobian is given by

$$\mathbf{G}(\boldsymbol{q}_n, \boldsymbol{q}_{n+1})^T = \left[\bar{\nabla}\Phi_1(\boldsymbol{q}_n, \boldsymbol{q}_{n+1}), \ldots, \bar{\nabla}\Phi_m(\boldsymbol{q}_n, \boldsymbol{q}_{n+1})\right] \tag{7}$$

Concerning (6), for the present purposes it suffices to set $\mathbf{Q}(\mathbf{q}_n,\ \mathbf{q}_{n+1}) = \mathbf{Q}(\mathbf{q}_{n+1/2})$. The BEM scheme can be used to determine $\mathbf{q}_{n+1} \in \mathbf{Q}$, $v_{n+1} \in \mathbb{R}^n$ and $\bar{\boldsymbol{\lambda}} \in \mathbb{R}^m$. To this end, one may substitute for v_{n+1} from $(5)_1$ into $(5)_2$ and then solve the remaining system of nonlinear algebraic equations for the $n + m$ unknowns $(\mathbf{q}_{n+1},\ \bar{\boldsymbol{\lambda}})$. We refer to [Bet05a] for further details of the implementation.

Remark 2.1 The algorithm (5) inherits fundamental mechanical properties from the underlying continuous formulation such as (i) conservation of energy, and (ii) conservation of momentum maps that are at most quadratic in $(\boldsymbol{q}, \boldsymbol{v})$. While algorithmic conservation of linear momentum is a trivial matter, algorithmic conservation of angular momentum and total energy is made possible by the specific formulation of rigid bodies and multibody systems proposed in the present work.

3. The planar rigid body

In the present work we make use of six redundant coordinates for the description of the placement of the planar rigid body. In particular, the vector of redundant coordinates is given by

$$\boldsymbol{q} = \begin{bmatrix} \boldsymbol{\varphi} \\ \boldsymbol{d}_1 \\ \boldsymbol{d}_2 \end{bmatrix} \tag{8}$$

where $\boldsymbol{\varphi} \in \mathbb{R}^2$ is the position vector of the center of mass and $\mathbf{d}_\alpha \in \mathbb{R}^2, \alpha \in \{1, 2\}$, are two directors which specify the orientation of the rigid body (Fig. 1). In the sequel, all of the coordinates in (8) are referred to a right-handed orthonormal basis $\{\mathbf{e}_1, \mathbf{e}_2\}$, which plays the role of an inertial frame. The directors are assumed to constitute a right-handed body frame which coincides with the principal axis of the rigid body. Since the directors are fixed in the body and moving with it, they have to stay orthonormal for all times $t \in \mathbb{R}^+$. This gives rise to three independent geometric (or holonomic) constraints $\boldsymbol{\phi}^i_{\text{int}}(\mathbf{q}) = 0$, which may be termed internal constraints since they are intimately connected with the assumption of rigidity. The functions $\boldsymbol{\phi}^i_{\text{int}} : \mathbb{R}^6 \to \mathbb{R}$ may be arranged in the vector of internal constraint functions

$$\boldsymbol{\Phi}_{int}(\boldsymbol{q}) = \begin{bmatrix} \frac{1}{2}[\boldsymbol{d}_1^T \boldsymbol{d}_1 - 1] \\ \frac{1}{2}[\boldsymbol{d}_2^T \boldsymbol{d}_2 - 1] \\ \boldsymbol{d}_1^T \boldsymbol{d}_2 \end{bmatrix} \tag{9}$$

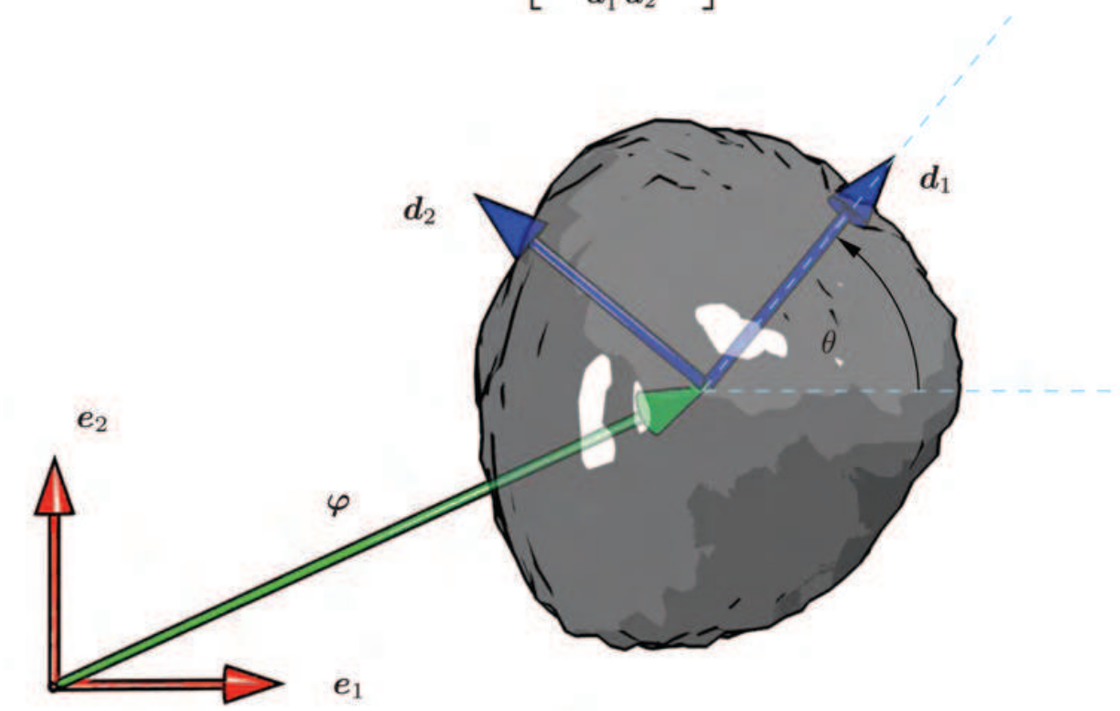

Figure 1: The planar rigid body.

With regard to the internal constraints the configuration space of the free rigid body may now be written in the form

$$\mathsf{Q}_{\text{free}} = \{\boldsymbol{q}(t) \in \mathbb{R}^6 \mid \boldsymbol{\Phi}_{int}(\boldsymbol{q}) = \boldsymbol{0}\,,\ (\boldsymbol{d}_1 \times \boldsymbol{d}_2) \cdot \boldsymbol{e}_3 = +1\} \tag{10}$$

Note that the director frame $\{\mathbf{d}_1, \mathbf{d}_2\}$ can be connected with a rotation matrix $\mathbf{R} \in$ SO(2), through the relationship $\mathbf{d}_\alpha = \mathbf{R}e_\alpha$. In this connection,

$$\mathrm{SO}(2) = \{\boldsymbol{R} \in \mathbb{R}^{2\times 2} \mid \boldsymbol{R}^T\boldsymbol{R} = \boldsymbol{I}_2\,,\ \det \boldsymbol{R} = +1\} \tag{11}$$

is the special orthogonal group of $\mathbb{R}^2$. Accordingly, $\mathbf{R}_{\alpha\beta} = e_\alpha \cdot d_\beta$, such that the directors coincide with the columns of the rotation matrix. Alternatively, the configuration space of the free rigid body may be written as

$$\mathsf{Q}_{\text{free}} = \mathbb{R}^2 \times \mathrm{SO}(2) \subset \mathbb{R}^6$$

The motion of the free rigid body can now be described by means of the DAEs (1). To this end, we have to provide the mass matrix $\mathbf{M} \in \mathbb{R}^{6\times 6}$, which is given by

$$\boldsymbol{M} = \begin{bmatrix} M\boldsymbol{I}_2 & \boldsymbol{0} & \boldsymbol{0} \\ \boldsymbol{0} & E_1\boldsymbol{I}_2 & \boldsymbol{0} \\ \boldsymbol{0} & \boldsymbol{0} & E_2\boldsymbol{I}_2 \end{bmatrix} \tag{12}$$

Here, M is the total mass of the rigid body and E_1, E_2 are the principal values of the Euler tensor relative to the center of mass. With respect to a reference configuration β with material points $\mathbf{X} = (\mathbf{X}_1, \mathbf{X}_2) \in \beta$ these quantities are given by

$$\begin{aligned} M &= \int_{\mathcal{B}} \varrho(X)\, d^2X \\ E_\alpha &= \int_{\mathcal{B}} (X_\alpha)^2 \varrho(X)\, d^2X \end{aligned} \tag{13}$$

where $\rho(\mathbf{X})$ is the local mass density. Note that E_1, E_2 can be related to the classical polar momentum of inertia about the center of mass, J, via the relationship

$$J = E_1 + E_2 \tag{14}$$

Furthermore, in view of the constraint functions (9), the constraint Jacobian pertaining to the free rigid body is given by $\mathbf{G}_{int} = D\,\boldsymbol{\Phi}_{int}(q)$. Thus

$$\boldsymbol{G}_{int}(\boldsymbol{q}) = \begin{bmatrix} \boldsymbol{0}^T & \boldsymbol{d}_1^T & \boldsymbol{0}^T \\ \boldsymbol{0}^T & \boldsymbol{0}^T & \boldsymbol{d}_2^T \\ \boldsymbol{0}^T & \boldsymbol{d}_2^T & \boldsymbol{d}_1^T \end{bmatrix} \tag{15}$$

To summarize, the motion of the planar free rigid body is governed by the DAEs (1), with n = 6 and m = 3. This rigid body formulation is the cornerstone of the present approach to the energy-momentum integration of arbitrary multibody systems. Additional details about the present rigid body formulation may be found in [BS01b,BL06].

4. Kinematic pairs

This section deals with basic kinematic pairs which are fundamental for building complex multibody systems. Here we will present the revolute and the prismatic pair which represent the basic pairs necessary to model common planar parallel manipulators. Within this chapter we will also introduce a specific coordinate augmentation technique for both pairs in order to incorporate joint variables into the present rigid body formulation.

4.1 The planar revolute pair

Each rigid body of the multibody system depicted in Fig. 2 is modelled as constrained mechanical system as described in Section 3. Accordingly, body A is characterized by 6 redundant coordinates

$$\boldsymbol{q}^A = \begin{bmatrix} \varphi^A \\ \boldsymbol{d}_1^A \\ \boldsymbol{d}_2^A \end{bmatrix} \tag{16}$$

along with internal constraints $\boldsymbol{\phi}_{\text{int}}^{A}(\mathbf{q}^{\text{A}}) \in \mathbb{R}^{3}$ of the form (9), associated constraint Jacobian $\mathbf{G}_{\text{int}}^{A}(\mathbf{q}^{\text{A}}) \in \mathbb{R}^{3\times 6}$ of the form (15), and mass matrix $\mathbf{M}^{\text{A}} \in \mathbb{R}^{6\times 6}$ of the form (12).

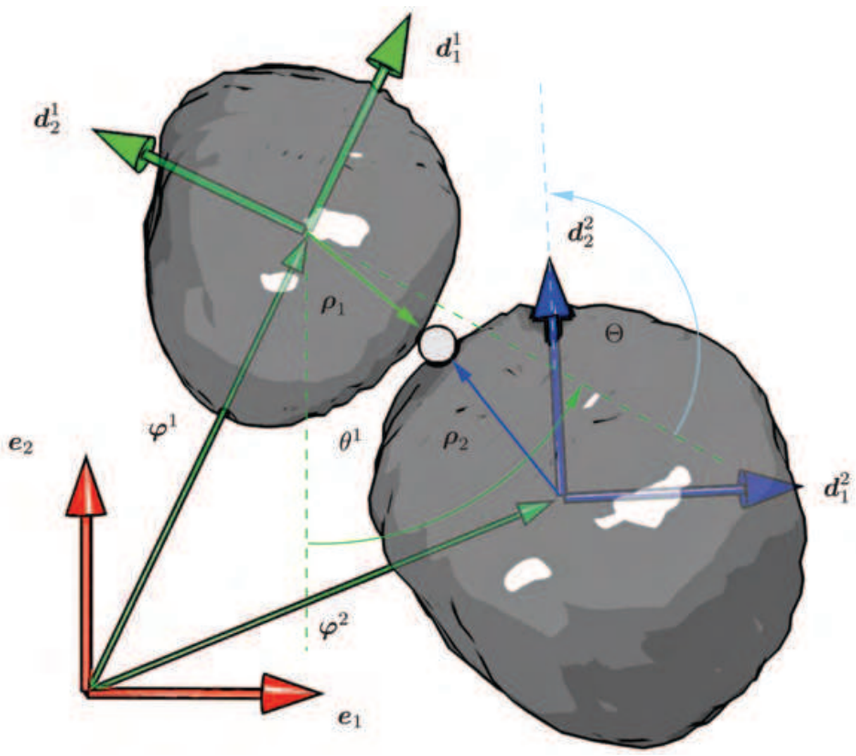

Figure 2: The planar revolute pair.

The description of the whole multibody system relies on the assembly of the individual bodies. The assembly procedure consists of the following steps. (i) The contributions of each individual body are collected in appropriate system vectors/matrices. For example, in the case of the present 2-body system (Fig. 2) we get the vector of redundant coordinates

$$\boldsymbol{q} = \begin{bmatrix} \boldsymbol{q}^1 \\ \boldsymbol{q}^2 \end{bmatrix} \tag{17}$$

along with the mass matrix

$$\boldsymbol{M} = \begin{bmatrix} \boldsymbol{M}^1 & \boldsymbol{0}_{6\times 6} \\ \boldsymbol{0}_{6\times 6} & \boldsymbol{M}^2 \end{bmatrix} \tag{18}$$

which, in view of (12), is diagonal and constant. Moreover, the constraints of rigidity are collected in the vector

$$\boldsymbol{\Phi}_{int} = \begin{bmatrix} \boldsymbol{\Phi}^1_{int} \\ \boldsymbol{\Phi}^2_{int} \end{bmatrix} \tag{19}$$

with corresponding constraint Jacobian

$$\boldsymbol{G}_{int} = \begin{bmatrix} \boldsymbol{G}^1_{int} & \boldsymbol{0}_{3\times 6} \\ \boldsymbol{0}_{3\times 6} & \boldsymbol{G}^2_{int} \end{bmatrix} \tag{20}$$

(ii) The interconnection between the rigid bodies in a multibody system is accounted for by external constraints.
For the revolute pair we get two additional constraint functions of the form

$$\boldsymbol{\Phi}_{ext}(\boldsymbol{q}) = \boldsymbol{\varphi}^2 - \boldsymbol{\varphi}^1 + \boldsymbol{\varrho}^2 - \boldsymbol{\varrho}^1 \tag{21}$$

where the vector

$$\boldsymbol{\varrho}^A = \sum_{\alpha=1}^{2} \varrho^A_\alpha \boldsymbol{d}^A_\alpha \tag{22}$$

specifies the position of the joint on body A. The constraints (21) give rise to the Jacobian

$$\boldsymbol{G}_{ext}(\boldsymbol{q}) = D\boldsymbol{\Phi}_{ext}(\boldsymbol{q}) = \begin{bmatrix} -\boldsymbol{I} & -\varrho^1_1\boldsymbol{I} & -\varrho^1_2\boldsymbol{I} & \boldsymbol{I} & \varrho^2_1\boldsymbol{I} & \varrho^2_2\boldsymbol{I} \end{bmatrix} \tag{23}$$

Accordingly, the present 2-body system is characterized by a total of m = 8 independent constraints

$$\boldsymbol{\Phi}(\boldsymbol{q}) = \begin{bmatrix} \boldsymbol{\Phi}_{int}(\boldsymbol{q}) \\ \boldsymbol{\Phi}_{ext}(\boldsymbol{q}) \end{bmatrix} \tag{24}$$

with corresponding 8×12 constraint Jacobian

$$\boldsymbol{G}(\boldsymbol{q}) = \begin{bmatrix} \boldsymbol{G}_{int}(\boldsymbol{q}) \\ \boldsymbol{G}_{ext}(\boldsymbol{q}) \end{bmatrix} \tag{25}$$

To summarize, the present description of the revolute pair makes use of n = 12 redundant coordinates subject to m = 8 constraints. This complies with the fact that the system at hand has $n - m$ = 4 degrees of freedom. Obviously, the configuration space of the revolute pair, Q_{revolute}, can be written in the form (4).

4.1.1 Discrete constraint Jacobian

Since the constraint functions in (24) are at most quadratic, the associated discrete derivative coincides with the mid-point evaluation of the continuous constraint Jacobian (25), i.e.

$$\mathbf{G}(\boldsymbol{q}_n, \boldsymbol{q}_{n+1}) = \boldsymbol{G}(\boldsymbol{q}_{n+\frac{1}{2}}) \tag{26}$$

4.1.2 Coordinate augmentation

In many practical applications rotational variables along with associated torques are required for the description of a multibody system. Although the present approach circumvents the use of rotational variables throughout the discretization procedure, rotations can be easily incorporated into the present method. To this end, we next propose a coordinate augmentation technique. The idea is to incorporate a joint torque into the revolute pair (Fig. 2). Therefore we extend the original configuration vector

$$\boldsymbol{q} = \begin{bmatrix} \boldsymbol{q}^1 \\ \boldsymbol{q}^2 \\ \Theta \end{bmatrix} \tag{27}$$

The new coordinate Θ is connected with the original ones by introducing an additional constraint function of the form

$$\Phi^R_{aug}(\boldsymbol{q}) = \boldsymbol{d}_2^2 \cdot \boldsymbol{d}_1^1 + \sin\Theta + \boldsymbol{d}_2^2 \cdot \boldsymbol{d}_2^1 - \cos\Theta \tag{28}$$

In anticipation of the subsequent treatment of the discretization we write (28) in partitioned form

$$\Phi^R_{aug}(\boldsymbol{q}) = \Phi^1_{aug}(\boldsymbol{q}_{ori}) + \Phi^2_{aug}(\Theta) \tag{29}$$

with the original coordinates

$$\boldsymbol{q}_{ori} = \begin{bmatrix} \boldsymbol{q}^1 \\ \boldsymbol{q}^2 \end{bmatrix} \tag{30}$$

and

$$\begin{aligned} \Phi^1_{aug}(\boldsymbol{q}_{ori}) &= \boldsymbol{d}_2^2 \cdot \boldsymbol{d}_1^1 + \boldsymbol{d}_2^2 \cdot \boldsymbol{d}_2^1 \\ \Phi^2_{aug}(\Theta) &= \sin\Theta - \cos\Theta \end{aligned} \tag{31}$$

Additionally, we get the Jacobian

$$\boldsymbol{G}_{aug}(\boldsymbol{q}) = D\Phi_{aug}(\boldsymbol{q}) = \begin{bmatrix} \boldsymbol{0}^T & \boldsymbol{d}_2^{2^T} & \boldsymbol{d}_2^{2^T} & \boldsymbol{0}^T & \boldsymbol{0}^T & (\boldsymbol{d}_1^1 + \boldsymbol{d}_2^1)^T & (\sin\Theta + \cos\Theta) \end{bmatrix} \tag{30}$$

With regard to (29), we decompose (32) according to

$$\boldsymbol{G}_{aug}(\boldsymbol{q}) = \begin{bmatrix} \boldsymbol{G}^1_{aug}(\boldsymbol{q}_{ori}) & G^2_{aug}(\Theta) \end{bmatrix} \tag{33}$$

with

$$\begin{aligned} \boldsymbol{G}^1_{aug}(\boldsymbol{q}_{ori}) &= \begin{bmatrix} \boldsymbol{0}^T & \boldsymbol{d}_2^{2^T} & \boldsymbol{d}_2^{2^T} & \boldsymbol{0}^T & \boldsymbol{0}^T & (\boldsymbol{d}_1^1 + \boldsymbol{d}_2^1)^T \end{bmatrix} \\ G^2_{aug}(\Theta) &= \sin\Theta + \cos\Theta \end{aligned} \tag{34}$$

To summarize, we now have n = 13 coordinates subject to m = 9 geometric constraints. In order to completely specify the DAEs (1) for the augmented system at hand one simply has to extend the relevant matrices of the revolute pair in Section 4.1. Accordingly, the mass matrix of the augmented system is given by

$$\boldsymbol{M} = \begin{bmatrix} \boldsymbol{M}^1 & \boldsymbol{0}_{6\times 6} & \boldsymbol{0}_{6\times 1} \\ \boldsymbol{0}_{6\times 6} & \boldsymbol{M}^2 & \boldsymbol{0}_{6\times 1} \\ \boldsymbol{0}_{1\times 6} & \boldsymbol{0}_{1\times 6} & 0 \end{bmatrix} \tag{35}$$

In view of (28), the augmentation gives rise to an extended vector of constraint functions of the form

$$\boldsymbol{\Phi}(\boldsymbol{q}) = \begin{bmatrix} \boldsymbol{\Phi}_{ori}(\boldsymbol{q}_{ori}) \\ \Phi_{aug}(\boldsymbol{q}) \end{bmatrix} \tag{36}$$

where ϕ_{ori} stands for the original constraints given by (24). The augmented constraint Jacobian assumes the form

$$\boldsymbol{G}(\boldsymbol{q}) = \begin{bmatrix} \boldsymbol{G}_{ori}(\boldsymbol{q}_{ori}) & \boldsymbol{0}_{8\times 1} \\ \boldsymbol{G}^1_{aug}(\boldsymbol{q}_{ori}) & G^2_{aug}(\Theta) \end{bmatrix} \tag{37}$$

where $\mathbf{G}_{\text{ori}}$ represents the original constraint Jacobian given by (25).

4.1.3 Discrete constraint Jacobian

The discrete version of (37) can be written as

$$\mathbf{G}(\boldsymbol{q}_n, \boldsymbol{q}_{n+1}) = \begin{bmatrix} \boldsymbol{G}_{ori}\big((\boldsymbol{q}_{ori})_{n+\frac{1}{2}}\big) & \boldsymbol{0}_{8\times 1} \\ \boldsymbol{G}^1_{aug}\big((\boldsymbol{q}_{ori})_{n+\frac{1}{2}}\big) & \mathrm{G}^2_{aug}(\Theta_n, \Theta_{n+1}) \end{bmatrix} \tag{38}$$

Since the constraint functions $\boldsymbol{\phi}_{\text{ori}}(\boldsymbol{q}_{\text{ori}})$ and $\boldsymbol{\phi}^{\,1}_{aug}(\boldsymbol{q}_{\text{ori}})$ (cf. (24) and $(31)_1$, respectively) are at most quadratic, the associated discrete gradient coincides with the mid-point evaluation of the respective continuous constraint Jacobians. This is in contrast to the constraint function $\boldsymbol{\phi}^{\,2}_{aug}(\Theta)$, see $(31)_2$. In this case we choose

$$\mathrm{G}^2_{aug}(\Theta_n, \Theta_{n+1}) = \frac{\Phi^2_{aug}(\Theta_{n+1}) - \Phi^2_{aug}(\Theta_n)}{\Theta_{n+1} - \Theta_n} \tag{39}$$

If

$$\Theta_{n+1} = \Theta_n, \text{ then } \mathrm{G}^2_{aug}(\Theta_n, \Theta_{n+1}) = \big(\Phi^2_{aug}\big)'(\Theta_n).$$

Remark 4.1 *Formula (39) can be interpreted as G-equivariant discrete derivative of the corresponding constraint function in the sense of Gonzalez [Gon96]. In this connection G represents the group acting by translations and rotations, respectively. In the present case (39) coincides with Greenspan's formula [Gre84].*

4.1.4 Numerical example

To demonstrate the numerical performance of the present formulation we investigate the free flight of our institute logo NM (*N*umerical *M*echanics[1]). Both letters are modelled as rigid bodies which are connected by a revolute joint. (Fig. 3).

The inertial parameters for the numerical example are summarized in Table 1. The location of the joint relative to each body is specified by (22) with

The inertial parameters for the numerical example are summarized in Table 1. The location of the joint relative to each body is specified by (22) with

$$[\varrho^1_\alpha] = \begin{bmatrix} 0 \\ -0.4 \end{bmatrix} \quad \text{and} \quad [\varrho^2_\alpha] = \begin{bmatrix} 0 \\ 0.4 \end{bmatrix} \tag{40}$$

[1] http://www.uni-siegen.de/fb11/nm

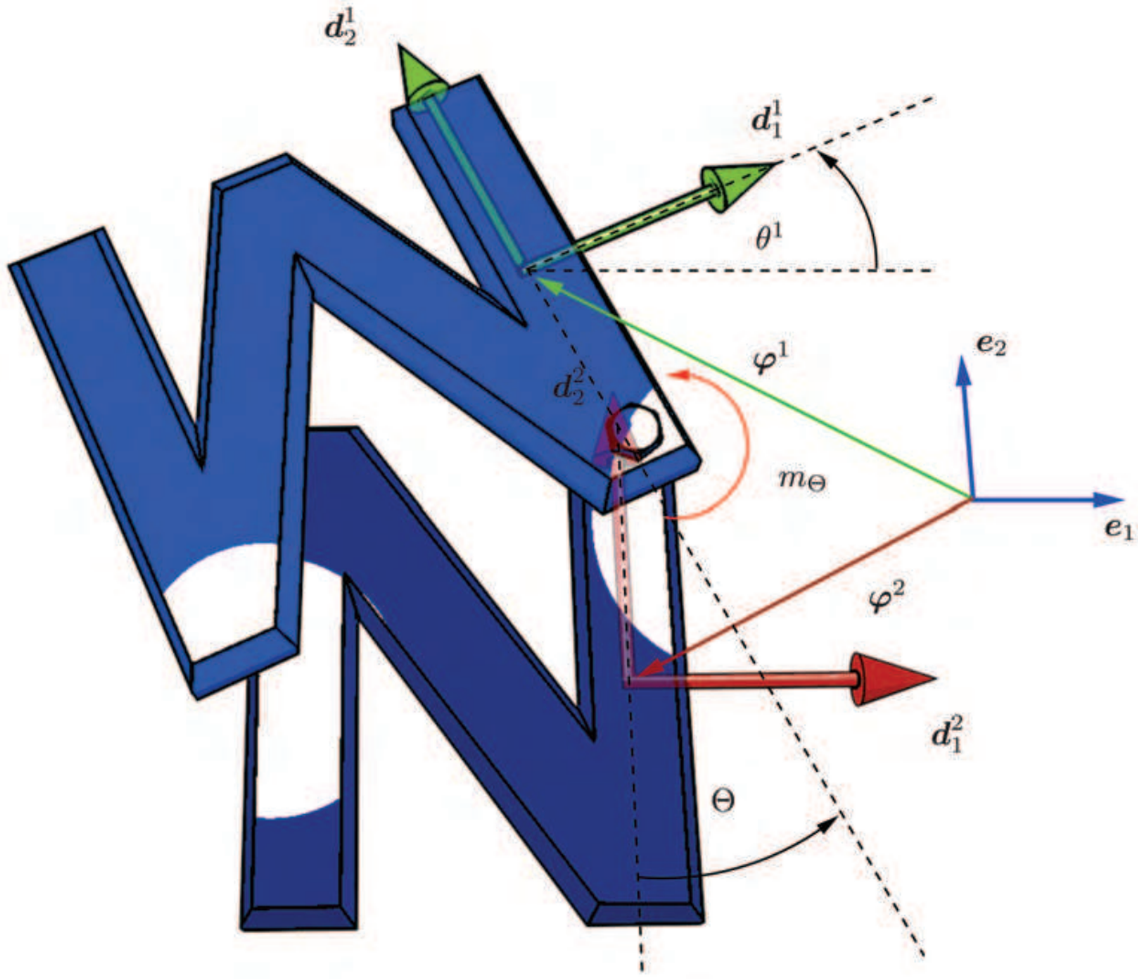

Figure 3: The NM-logo as 2-body system. Arbitrary configuration of both connected letters.

The initial configuration of the system is given by the following generalized coordinates (see Fig. 3)

$$\boldsymbol{u}_0 = \begin{bmatrix} \boldsymbol{\varphi}_0^1 \\ \theta_0^1 \\ \Theta_0 \end{bmatrix} = \begin{bmatrix} \mathbf{0} \\ 0 \\ \pi \end{bmatrix} \tag{41}$$

Initial generalized velocities can be written as

$$\boldsymbol{\nu}_0 = \begin{bmatrix} \boldsymbol{e}_1 \cdot (\boldsymbol{v}_\varphi^1)_0 \\ \boldsymbol{e}_2 \cdot (\boldsymbol{v}_\varphi^1)_0 \\ \omega_0^1 \\ \dot{\Theta}_0 \end{bmatrix} \tag{42}$$

In the present example the system is initially at rest, i.e. $\nu_0 = 0$. Since it is a free flight, we neglect the gravitational forces, having no potential energy in the system. To initialize the motion, external loads $\mathbf{Q} \in R^{13}$ are acting on the system. Specifically,

$$\boldsymbol{Q} = \begin{bmatrix} \mathbf{0}_{12\times 1} \\ m_\Theta(t) \end{bmatrix} \tag{43}$$

This means that we only apply an external joint torque, which is directly acting on the newly introduced rotational component Θ. The torque itself is applied in the form of a hat function over time (cf. Fig. 4), where $t_1 = 0.25$, $t_2 = 0.5$, $\bar{m} = 5$. Accordingly, for $t > t_2$ no external forces act on the system anymore. The system can thus be classified as an autonomous Hamiltonian system with symmetry. Consequently, the Hamiltonian (or the total energy) represents a conserved quantity for $t > t_2$. The angular momentum remains equal for all times, since it is an internal joint torque acting on the system. The present energy-momentum scheme does indeed satisfy these conservation properties for any time step Δt, see Fig. 5. The simulated motion is illustrated with some snapshots at discrete times in Fig. 6. Moreover, the evolution of the angle $\Theta(t)$, calculated with different time steps $\Delta t \in \{0.1, 0.05, 0.01\}$, is depicted in Fig. 7.

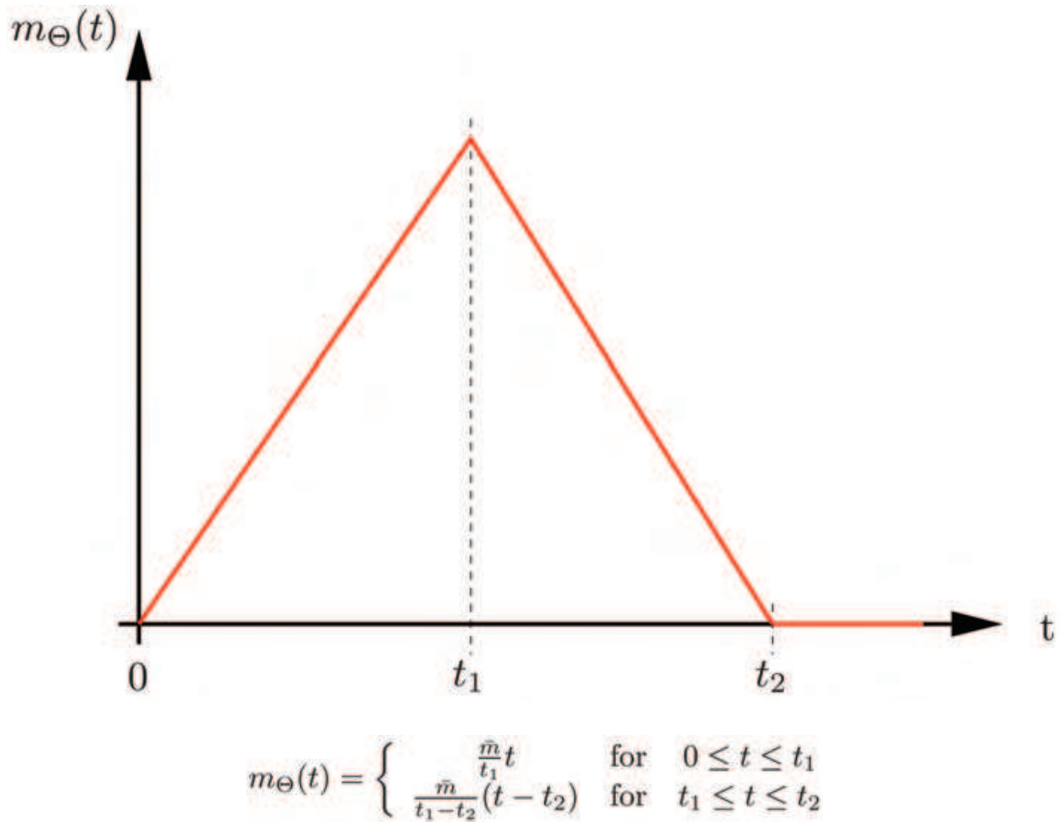

Figure 4: Magnitude of the torque during the initial load period.

body	M	E_1	E_2
1	1.1	0.004	0.0917
2	2	0.0073	0.1667

Table 1: Inertial parameters for the 2-body system.

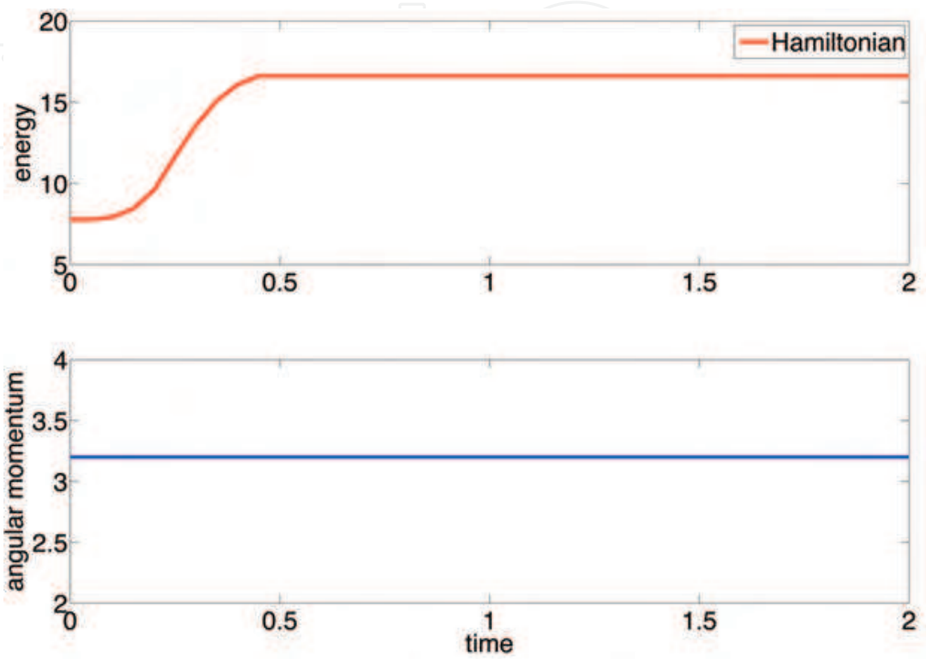

Figure 5: Algorithmic conservation of energy and angular momentum, $\Delta t = 0.05$.

Figure 6: Snapshots of the free flying NM-logo. The two curves correspond to the trajectories of the mass centers of the individual bodies constituting the present multibody system ($t \in \{0, 1, 2\}$s).

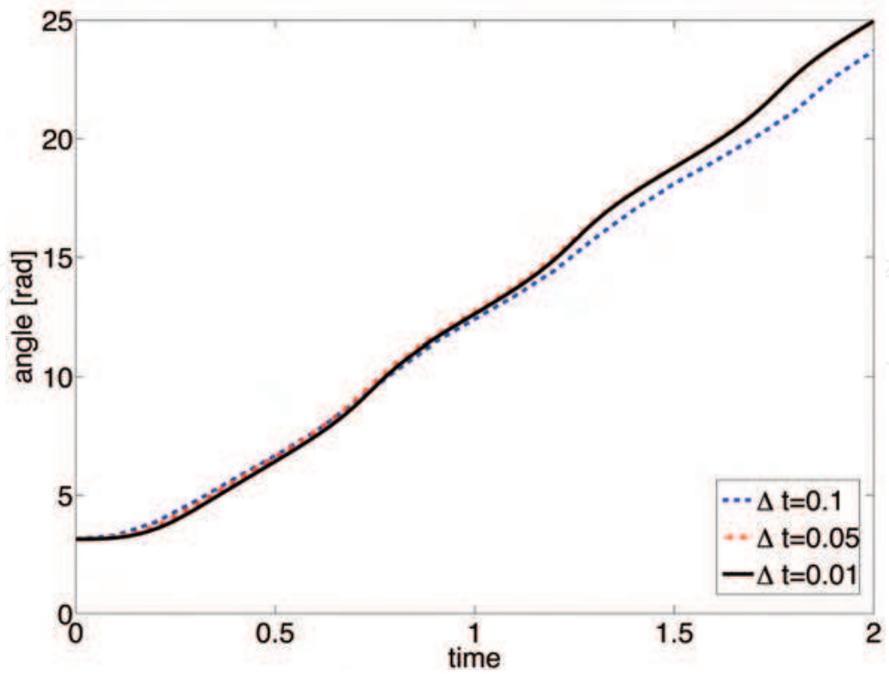

Figure 7: Angle Θ (t) over time.

4.2 The planar prismatic pair

Analogous to the previously presented revolute pair, we now focus on the prismatic pair. The procedure is similar to the prismatic pair, we will present the necessary constraints and their Jacobians. A coordinate augmentation for the prismatic pair will measure the distance between both rigid bodies. The example will deal with a planar linear motion guide.

The prismatic pair (Fig. 8) will again be considered as a constrained mechanical systems. Since the number of bodies and their internal description corresponds to the revolute pair, the configuration vector (17), the mass matrix (18) and the internal constraints as well as their Jacobians (19), (20) have the same structure as already presented for the revolute pair. The interconnection between both bodies characterizes the prismatic joint and can be written as:

$$\boldsymbol{\Phi}_{ext}(\boldsymbol{q}) = \begin{bmatrix} (\boldsymbol{m}^1) \cdot (\boldsymbol{p}^2 - \boldsymbol{p}^1) \\ \boldsymbol{d}_1^1 \cdot \boldsymbol{d}_2^2 - \eta \end{bmatrix} \tag{44}$$

with the vectors

$$\boldsymbol{m} = \sum_{\alpha=1}^{2} m_\alpha \boldsymbol{d}_\alpha^1 \quad \text{and} \quad \boldsymbol{p}^i = \boldsymbol{\varphi}^i + \boldsymbol{\rho}^i \tag{45}$$

The vector $\boldsymbol{\rho}^i$ has already been defined in eq. (22). The value of η in (44) needs to be prescribed initially. The corresponding constraint Jacobian yields:

$$\boldsymbol{G}_{ext}(\boldsymbol{q}) = \begin{bmatrix} -(\boldsymbol{m})^T & \boldsymbol{G}_1^1 & \boldsymbol{G}_2^1 & (\boldsymbol{m})^T & \rho_1^2(\boldsymbol{m})^T & \rho_2^2(\boldsymbol{m})^T \\ \boldsymbol{0}^T & (\boldsymbol{d}_2^2)^T & \boldsymbol{0}^T & \boldsymbol{0}^T & \boldsymbol{0}^T & (\boldsymbol{d}_1^1)^T \end{bmatrix} \tag{46}$$

with

$$\boldsymbol{G}_i^1 = m_i(\boldsymbol{p}^2 - \boldsymbol{p}^1)^T - \rho_i^1(\boldsymbol{m})^T \quad \text{for} \quad i = 1, 2 \tag{47}$$

This leads again to m = 8 independent constraints, the global constraint Jacobian has the form of eq. (25). The number of unknowns is the same as for the revolute pair, since we only have one relative coordinate between both bodies (u).

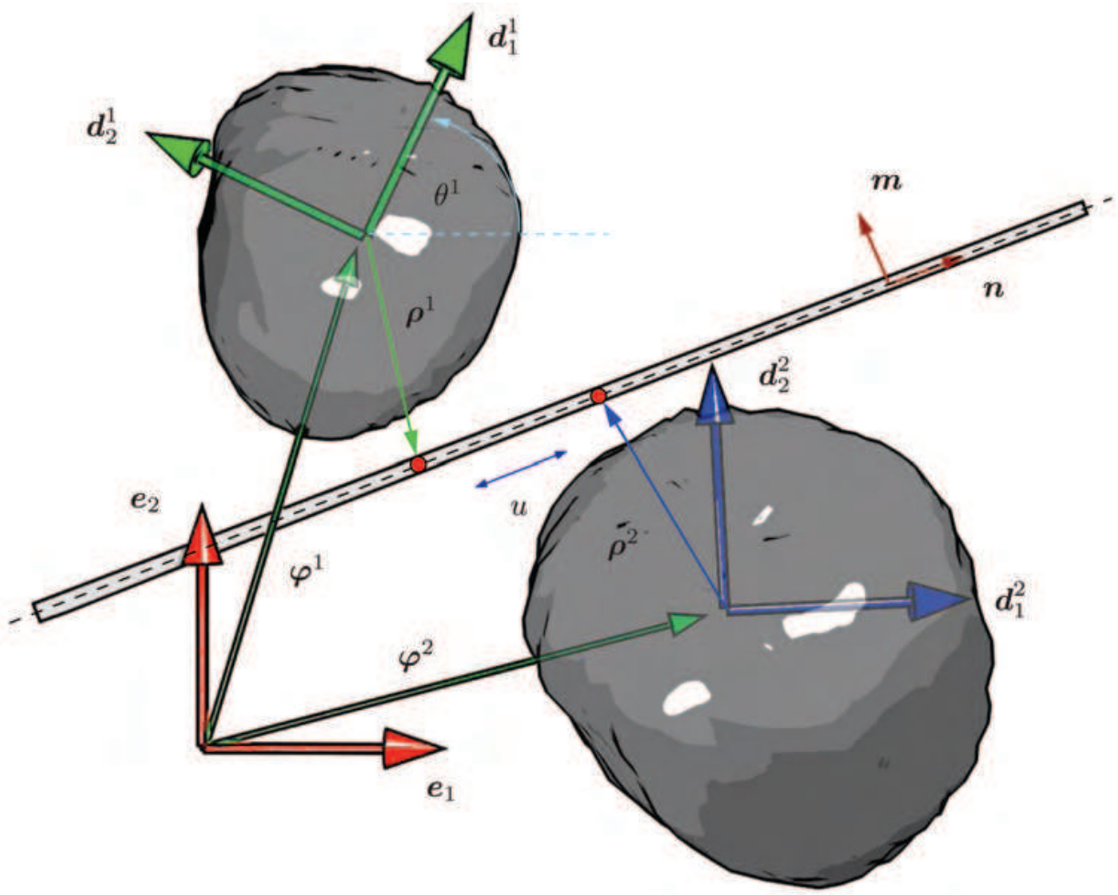

Figure 8: The planar prismatic pair.

4.2.1 Discrete constraint Jacobian

A closer investigation of (44) reveals that the constraint functions are quadratic, which means that the discrete derivative coincides with the mid-point evaluation of the constraint Jacobian (46). Therefore the discrete version of the constraint Jacobian is given by:

$$\mathbf{G}(\boldsymbol{q}_n, \boldsymbol{q}_{n+1}) = \boldsymbol{G}(\boldsymbol{q}_{n+\frac{1}{2}})$$

4.2.2 Coordinate augmentation

As already outlined for the revolute pair, for practical issues it is vital to incorporate augmented values into our rotationless formulation for multibody systems. Similar to the introduction of a relative angle for the revolute pair, we now account for the translational displacement between both rigid bodies. This time we will augment the system by the variable u which represents a generalized coordinate measuring the distance between the center of masses of both bodies.

Accordingly we start with the extension of our configuration vector by the new coordinate:

$$\boldsymbol{q} = \begin{bmatrix} \boldsymbol{q}^1 \\ \boldsymbol{q}^2 \\ u \end{bmatrix} = \begin{bmatrix} \boldsymbol{q}_{ori} \\ u \end{bmatrix} \tag{49}$$

The incorporation of a new redundant coordinate needs also a corresponding constraint. In this case we can write:

$$\Phi^P_{aug}(\boldsymbol{q}) = (\boldsymbol{p}^2 - \boldsymbol{p}^1) \cdot \boldsymbol{n} - u \tag{50}$$

As outlined before, **n** represents the axis of sliding and can also be described as

$$\boldsymbol{n} = \sum_{\alpha=1}^{2} n_\alpha \boldsymbol{d}^1_\alpha \tag{51}$$

Again we decompose the constraint vector in two parts. One depending on the original coordinates and a second one depending on the newly introduced coordinate u

$$\Phi^P_{aug}(\boldsymbol{q}) = \Phi^1_{aug}(\boldsymbol{q}_{ori}) + \Phi^2_{aug}(u) \tag{52}$$

The same will be done with its corresponding constraint Jacobian:

$$\boldsymbol{G}_{aug}(\boldsymbol{q}) = \begin{bmatrix} \boldsymbol{G}^1_{aug}(\boldsymbol{q}_{ori}) & G^2_{aug}(u) \end{bmatrix} \tag{53}$$

For both parts we obtain:

$$\begin{array}{rcl} \boldsymbol{G}^1_{aug}(\boldsymbol{q}_{ori}) & = & \begin{bmatrix} -\boldsymbol{n}^T & n_1(\boldsymbol{p}^2 - \boldsymbol{p}^1)^T - \rho^1_1 \boldsymbol{n}^T & n_2(\boldsymbol{p}^2 - \boldsymbol{p}^1)^T - \rho^1_2 \boldsymbol{n}^T & \boldsymbol{n}^T & \rho^2_1 \boldsymbol{n}^T & \rho^2_2 \boldsymbol{n}^T \end{bmatrix} \\ G^2_{aug}(u) & = & -1 \end{array} \tag{54}$$

As already presented in section (4.1.2), extending the configuration vector means also to expand the mass matrix (35) and the global constraint Jacobian (37). These steps are equivalent to the revolute pair.

4.2.3 Discrete constraint Jacobian

The discrete version of (37) for the prismatic pair can be written as

$$\mathbf{G}(\boldsymbol{q}_n, \boldsymbol{q}_{n+1}) = \begin{bmatrix} \boldsymbol{G}_{ori}\big((\boldsymbol{q}_{ori})_{n+\frac{1}{2}}\big) & \mathbf{0}_{8\times 1} \\ \boldsymbol{G}^1_{aug}\big((\boldsymbol{q}_{ori})_{n+\frac{1}{2}}\big) & \mathrm{G}^2_{aug}(u_{n+\frac{1}{2}}) \end{bmatrix} \tag{55}$$

Since the augmented constraint is at most quadratic, a simple mid-point evaluation is sufficient.

body	M	E_1	E_2	Length	Width
1	1.1	0.0229	5.8667	8	0.5
2	2	0.1667	0.1667	1	1

Table 2: Inertial parameters for the prismatic 2-body system.

4.2.4 Numerical example

In order to demonstrate the performance of the prismatic pair, we consider a linear motion guide (Fig. 9). It consists of two rigid bodies connected via a prismatic joint. The pair moves freely with given initial velocities in space.

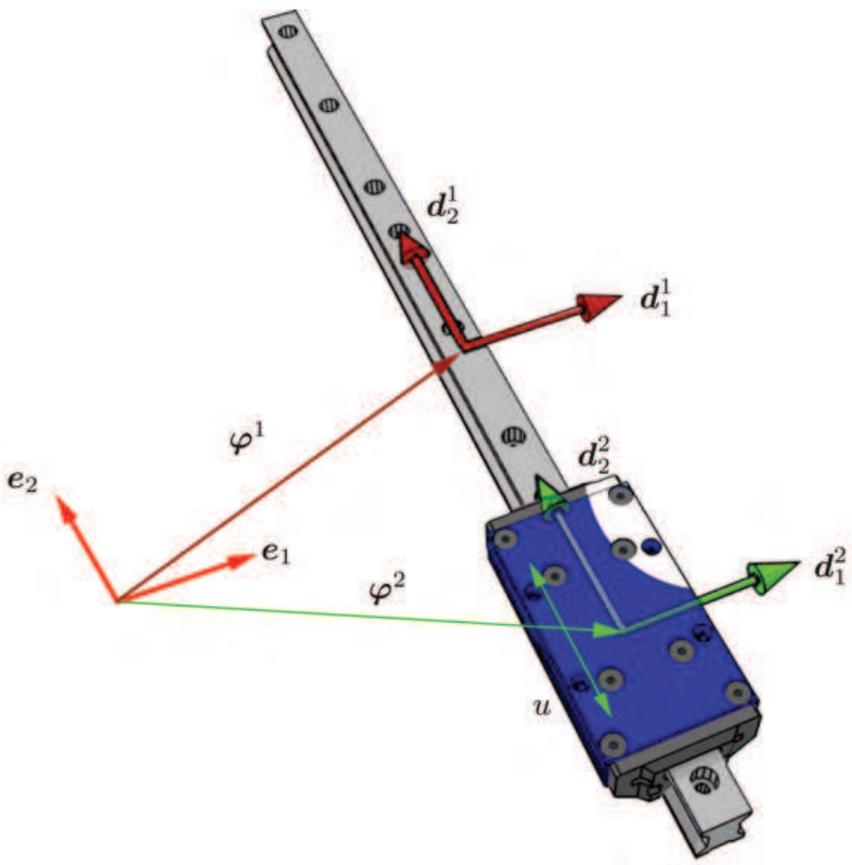

Figure 9: The linear motion guide as a 2 body system.

The inertial parameters for the numerical example are summarized in Table 2. The initial configuration of the system is given by (cf. Section 4.2 and Fig. 8):

$$\boldsymbol{u}_0 = \begin{bmatrix} \boldsymbol{\varphi}_0^1 \\ \theta_0^1 \\ u_0 \end{bmatrix} = \begin{bmatrix} \mathbf{0} \\ 0 \\ -3 \end{bmatrix} \tag{56}$$

Initial velocities can again be set in a generalized form:

$$\boldsymbol{\nu}_0 = \begin{bmatrix} \boldsymbol{e}_1 \cdot (\boldsymbol{v}_\varphi^1)_0 \\ \boldsymbol{e}_2 \cdot (\boldsymbol{v}_\varphi^1)_0 \\ \omega_0^1 \\ \dot{u}_0 \end{bmatrix} = \begin{bmatrix} 4 \\ 1 \\ \pi/2 \\ -6.5 \end{bmatrix} \tag{57}$$

Since there are no loads applied on the system, the total energy (Hamiltonian) and the angular momentum shall be conserved quantities. Once again the present energy-momentum scheme does indeed satisfy these conservation properties for any time step Δt, see Fig. 10. Some specific positions of the motion are displayed in Fig. 11. The evolution of the augmented coordinate u for different time steps $\Delta t \in \{0.1, 0.05, 0.01\}$, is depicted in Fig. 12.

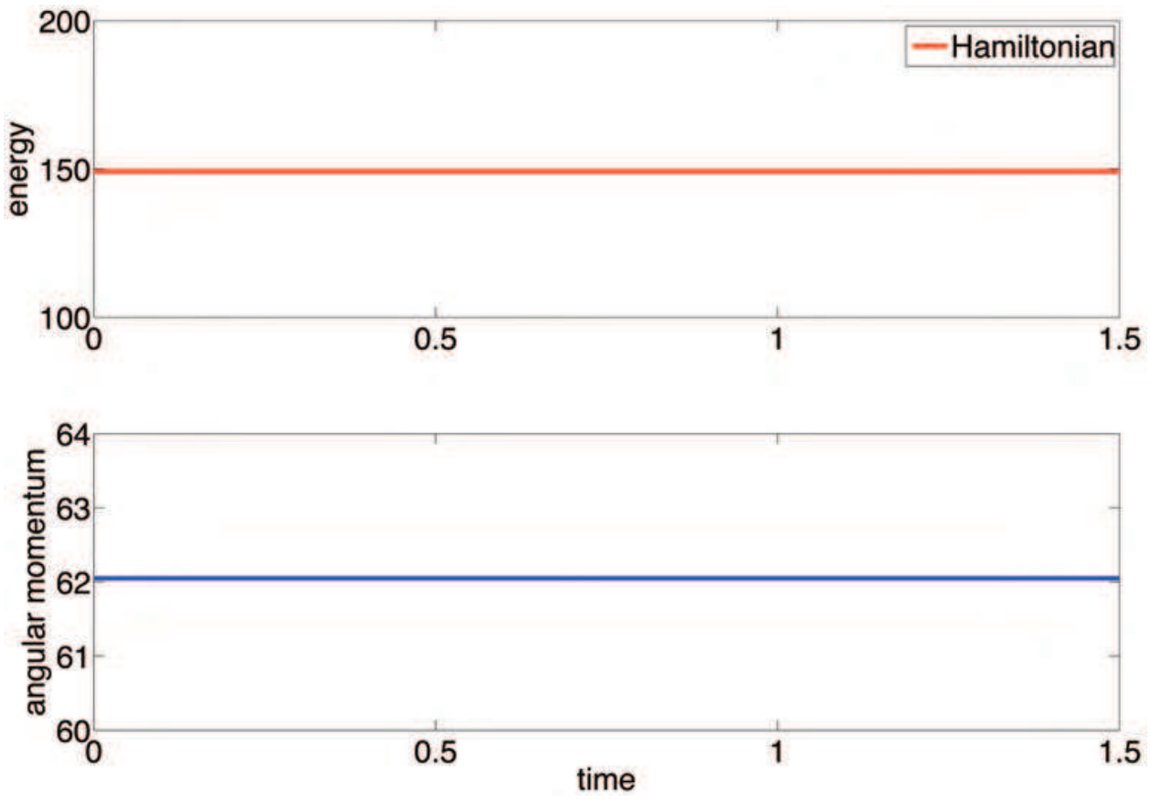

Figure 10: Algorithmic conservation of energy and angular momentum, $\Delta t = 0.1$.

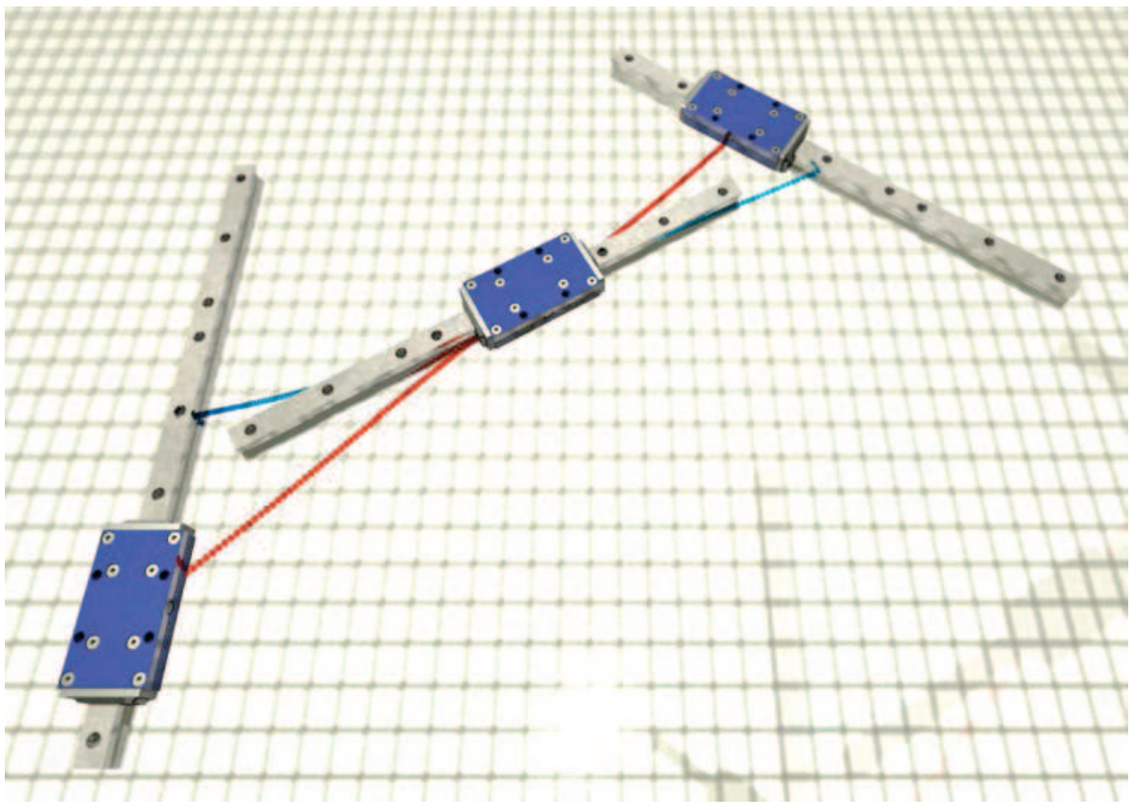

Figure 11: Snapshots of the free flight of the prismatic pair. Trajectories mark the movement of the center of masses ($t \in \{0, 0.8, 1.5\}$s).

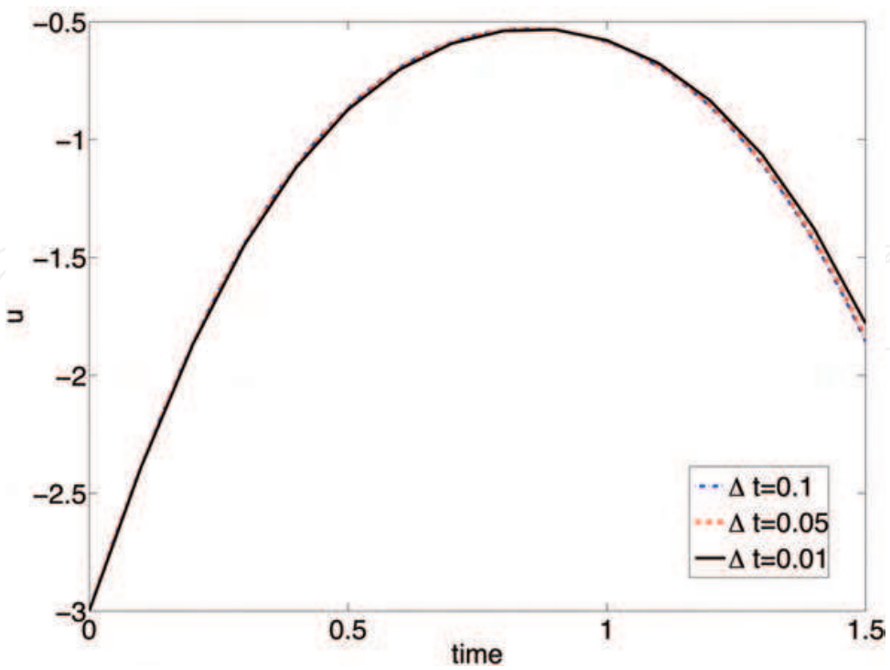

Figure 12: Translational displacement u over time.

5. Planar parallel manipulator

In this section we will combine all previous features in the example of a planar parallel manipulator. Since we have presented the revolute and prismatic pair, we will build a model of a RPR-manipulator, where the letters mark the kind of joints the mechanism consists of (**R**evolute-**P**rismatic-**R**evolute). The Figure below shows the configuration of the RPR-manipulator:

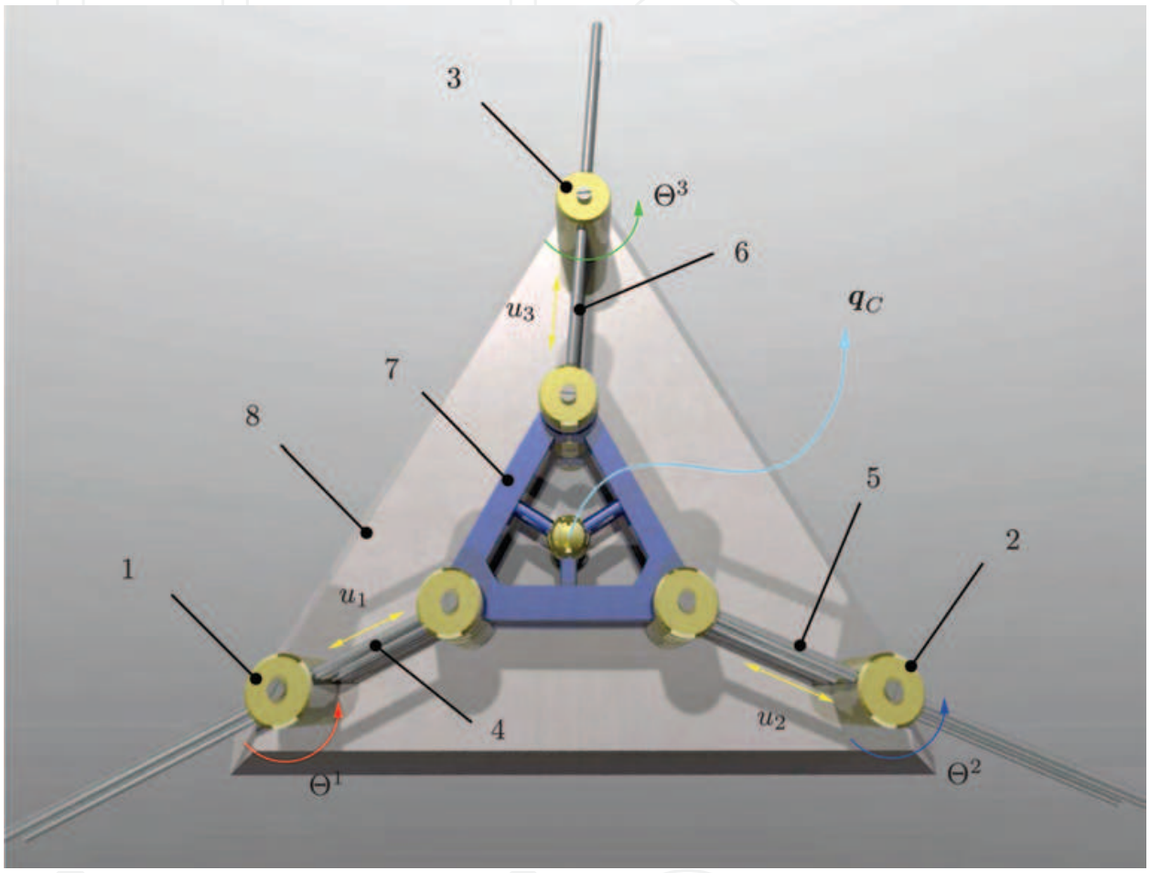

Figure 13: Schematics of the RPR-manipulator.

The goal in this example is to perform a controlled motion (vector $\mathbf{q}_C$ in upper Figure) of the inner triangle (body 7). Therefore we need to augment our original BEM-scheme (1) by control constraints and their corresponding constraint Jacobian. The enhanced continuous DAE structure yields to:

$$\begin{aligned} \dot{\boldsymbol{q}} - \boldsymbol{v} &= \mathbf{0} \\ \boldsymbol{M}\dot{\boldsymbol{v}} - \boldsymbol{F} + \boldsymbol{G}^T\boldsymbol{\lambda} + \boldsymbol{B}^T\bar{\boldsymbol{m}} &= \mathbf{0} \\ \boldsymbol{\Phi}(\boldsymbol{q}) &= \mathbf{0} \\ \boldsymbol{\Phi}_{\boldsymbol{C}}(\boldsymbol{q}) &= \mathbf{0} \end{aligned} \tag{58}$$

Here $\boldsymbol{\phi}_C(\mathbf{q})$ accounts for the newly introduced control constraints. Their corresponding Jacobian is $\mathbf{B}$, while its product with $\bar{\boldsymbol{m}}$ represents the necessary control forces.

A direct discretization of the equations above leads to an enhanced BEM-scheme for the presented underactuated system:

$$\begin{aligned} \boldsymbol{q}_{n+1} - \boldsymbol{q}_n &= \frac{\Delta t}{2}\left(\boldsymbol{v}_n + \boldsymbol{v}_{n+1}\right) \\ \boldsymbol{M}\left(\boldsymbol{v}_{n+1} - \boldsymbol{v}_n\right) &= \Delta t \mathbf{F}(\boldsymbol{q}_n, \boldsymbol{q}_{n+1}) - \Delta t \mathbf{G}(\boldsymbol{q}_n, \boldsymbol{q}_{n+1})^T \bar{\boldsymbol{\lambda}} - \Delta t \mathbf{B}(\boldsymbol{q}_n, \boldsymbol{q}_{n+1})^T \bar{\boldsymbol{m}} \\ \boldsymbol{\Phi}(\boldsymbol{q}_{n+1}) &= \mathbf{0} \\ \boldsymbol{\Phi}_C(\boldsymbol{q}_{n+1}) &= \mathbf{0} \end{aligned} \tag{59}$$

5.1 Rotationless formulation for the RPR manipulator

Here we will present the rotationless formulation for the RPR manipulator. The incorporation of rotational redundant coordinates plays a crucial role for the desired control problem. Additionally, as already presented in the sections before, we will also introduce translational redundant coordinates which measure the movement of the prismatic pairs. The mechanism presented herein consists of 8 rigid bodies. Bodies 1, 2 and 3 are connect via revolute joints to the free floating platform (body 8). The connection between body 1, 2, 3 and 4, 5, 6 is established by prismatic pairs. Finally 4, 5 and 6 are connected to the small triangle (body 7) via revolute joints. This structure consists of two closed loops, which means to formulate corresponding loop-closure constraints. The system at hand can then be characterized by the following configuration vector:

$$\boldsymbol{q}_{ori} = \begin{bmatrix} \boldsymbol{q}^1 \\ \boldsymbol{q}^2 \\ \boldsymbol{q}^3 \\ \boldsymbol{q}^4 \\ \boldsymbol{q}^5 \\ \boldsymbol{q}^6 \\ \boldsymbol{q}^7 \\ \boldsymbol{q}^8 \end{bmatrix}_{48\times 1} \quad \text{where} \quad \boldsymbol{q}_I = \begin{bmatrix} \boldsymbol{\varphi}^I \\ \boldsymbol{d}_1^I \\ \boldsymbol{d}_2^I \end{bmatrix} \quad \text{with} \quad I = 1, 2, ..., 8 \tag{60}$$

The upper vector has a size of 48, having eight rigid bodies means to invoke another m_{int} = 18 internal constraints and having nine joints at hand leads to m_{ext} = 24 external constraints. The difference n - m_{int} - m_{ext} = 6 means that the system at hand has a total of 6 DOF, since the platform (body 8) moves completely free and the inner triangle has another three DOF.
The necessary constraints for building the individual joints can be directly derived from chapter 4.1 and 4.2. This leads automatically to the closure of both loops. Here we neglect a detailed description of each individual joint and their constraint Jacobians, and only refer to the two previous chapters.

5.2 Coordinate augmentation

We now focus on the augmentation technique which is vital for the present application. As already outlined for both pairs (4.1 and 4.2), we incorporate rotational DOF (relative angles in-between body 8 and body 1, 2, 3) as well as translational DOF (distance between center of mass of body 1, 2, 3 and 4, 5, 6).

5.2.1 Rotational DOF

As indicated in Fig. 13, the first three joints of the parallel manipulator (with corresponding joint-rates $\dot{\Theta}^1$, $\dot{\Theta}^2$ and $\dot{\Theta}^3$) are actuated. To incorporate into the underlying rotationless formulation the possibility of imposing joint-torques ($\overline{m}_1$, $\overline{m}_2$, $\overline{m}_3$), we apply the coordinate augmentation technique proposed in Section 4.1.2. Indeed, the application of the coordinate augmentation technique to the present closed-loop system follows from a straight-forward extension of the treatment of the revolute pair in Section 4.1.

Similar to (27), we augment the originally used redundant coordinates $\mathbf{q}_{\text{ori}} \in \mathbb{R}^{48}$ with the joint-angles

$$\boldsymbol{\Theta} = \begin{bmatrix} \Theta^1 \\ \Theta^2 \\ \Theta^3 \end{bmatrix} \tag{61}$$

such that the augmented configuration vector reads

$$\boldsymbol{q} = \begin{bmatrix} \boldsymbol{q}_{ori} \\ \boldsymbol{\Theta} \end{bmatrix} \tag{62}$$

Accordingly, we now have $n = 51$ redundant coordinates. The three additional coordinates (61) are linked to the original ones through the introduction of three additional constraint functions. Similar to (36), the extended vector of constraint functions reads

$$\boldsymbol{\Phi}(\boldsymbol{q}) = \begin{bmatrix} \boldsymbol{\Phi}_{ori}(\boldsymbol{q}) \\ \boldsymbol{\Phi}_{aug}(\boldsymbol{q}) \end{bmatrix} \tag{63}$$

where, similar to (29), the additional constraints are specified by

$$\boldsymbol{\Phi}_{aug}(\boldsymbol{q}) = \boldsymbol{\Phi}^{I}_{aug}(\boldsymbol{q}_{ori}) + \boldsymbol{\Phi}^{II}_{aug}(\boldsymbol{\Theta}) \tag{64}$$

where

$$\boldsymbol{\Phi}^{I}_{aug}(\boldsymbol{q}_{ori}) = \begin{bmatrix} \left(\Phi^{I}_{aug}\right)_1 \\ \left(\Phi^{I}_{aug}\right)_2 \\ \left(\Phi^{I}_{aug}\right)_3 \end{bmatrix} \quad \text{with} \quad \left(\Phi^{I}_{aug}\right)_j = \boldsymbol{d}^{j}_{2} \cdot \left(\boldsymbol{d}^{8}_{1} + \boldsymbol{d}^{8}_{2}\right) \tag{65}$$

and

$$\boldsymbol{\Phi}^{II}_{aug}(\boldsymbol{\Theta}) = \begin{bmatrix} \left(\Phi^{II}_{aug}\right)\left(\Theta^1\right) \\ \left(\Phi^{II}_{aug}\right)\left(\Theta^2\right) \\ \left(\Phi^{II}_{aug}\right)\left(\Theta^3\right) \end{bmatrix} \quad \text{with} \quad \left(\Phi^{II}_{aug}\right)\left(\Theta^j\right) = \sin\Theta^j - \cos\Theta^j \tag{66}$$

We thus have a total of $m = 45$ constraints. Consequently, the BEM scheme relies on $n + m = 96$ unknowns. Similar to (37), the augmented constraint Jacobian is given by

$$\boldsymbol{G}(\boldsymbol{q}) = \begin{bmatrix} \boldsymbol{G}_{ori}(\boldsymbol{q}_{ori}) & \boldsymbol{0}_{48\times 3} \\ \boldsymbol{G}^{I}_{aug}(\boldsymbol{q}_{ori}) & \boldsymbol{G}^{II}_{aug}(\boldsymbol{\Theta}) \end{bmatrix} \tag{67}$$

The 3×48 matrix $\mathbf{G}^{I}_{aug}(\mathbf{q}_{\text{ori}})$ has the same structure as $(34)_1$, and $\mathbf{G}^{II}_{aug}(\boldsymbol{\Theta})$ is given by

$$\boldsymbol{G}^{II}_{aug} = \begin{bmatrix} \sin\Theta^1 + \cos\Theta^1 & 0 & 0 \\ 0 & \sin\Theta^2 + \cos\Theta^2 & 0 \\ 0 & 0 & \sin\Theta^3 + \cos\Theta^3 \end{bmatrix} \tag{68}$$

Similar to (55) the discrete counterpart of (67) can be written in the form

$$\boldsymbol{G}(\boldsymbol{q}_n, \boldsymbol{q}_{n+1}) = \begin{bmatrix} \boldsymbol{G}_{ori}\left((\boldsymbol{q}_{ori})_{n+\frac{1}{2}}\right) & \boldsymbol{0}_{48\times 3} \\ \boldsymbol{G}^{I}_{aug}\left((\boldsymbol{q}_{ori})_{n+\frac{1}{2}}\right) & \boldsymbol{G}^{II}_{aug}(\boldsymbol{\Theta}_n, \boldsymbol{\Theta}_{n+1}) \end{bmatrix} \tag{69}$$

Here, the discrete version of (68) assumes the form

$$\boldsymbol{G}^{II}_{aug}(\boldsymbol{\Theta}_n, \boldsymbol{\Theta}_{n+1}) = \begin{bmatrix} G^{II}_{aug}(\Theta^1_n, \Theta^1_{n+1}) & 0 & 0 \\ 0 & G^{II}_{aug}(\Theta^2_n, \Theta^2_{n+1}) & 0 \\ 0 & 0 & G^{II}_{aug}(\Theta^3_n, \Theta^3_{n+1}) \end{bmatrix} \tag{70}$$

with

$$G^{II}_{aug}(\alpha, \beta) = \begin{cases} \dfrac{\left(\Phi^{II}_{aug}\right)(\beta) - \left(\Phi^{II}_{aug}\right)(\alpha)}{\beta - \alpha} & \text{if} \quad \alpha \neq \beta \\ \left(\Phi^{II}_{aug}\right)'(\alpha) & \text{if} \quad \alpha = \beta \end{cases} \tag{71}$$

5.2.2 Translational DOF

As already outlined for the prismatic pair in section 4.2.2, we apply the coordinate augmentation technique to incorporate translational DOF in the prismatic connection for the RPR manipulator. This means that additionally to the angle augmentation, we again augment the configuration vector by another three redundant coordinates:

$$\boldsymbol{u} = \begin{bmatrix} u^1 \\ u^2 \\ u^3 \end{bmatrix} \tag{72}$$

taking into account the augmented part from section 5.2.1 such that the new augmented configuration vector reads

$$\boldsymbol{q} = \begin{bmatrix} \boldsymbol{q}_{ori} \\ \boldsymbol{\Theta} \\ \boldsymbol{u} \end{bmatrix} \tag{73}$$

Thus the number of redundant coordinates raises to n = 54. Once again, the new redundant coordinates require additional constraint functions. Similar to (64), the constraint functions are specified by

$$\boldsymbol{\Phi}_{aug}(\boldsymbol{q}) = \boldsymbol{\Phi}^{I}_{aug}(\boldsymbol{q}_{ori}) + \boldsymbol{\Phi}^{II}_{aug}(\boldsymbol{u}) \tag{74}$$

where

$$\boldsymbol{\Phi}^{I}_{aug}(\boldsymbol{q}_{ori}) = \begin{bmatrix} \left(\Phi^{I}_{aug}\right)_1 \\ \left(\Phi^{I}_{aug}\right)_2 \\ \left(\Phi^{I}_{aug}\right)_3 \end{bmatrix} \quad \text{with} \quad \left(\Phi^{I}_{aug}\right)_j = \left(\boldsymbol{\varphi}^k - \boldsymbol{\varphi}^j\right) \cdot \boldsymbol{d}^j_2 \quad \text{with} \quad k = 4,5,6 \tag{75}$$

and

$$\boldsymbol{\Phi}^{II}_{aug}(\boldsymbol{u}) = \begin{bmatrix} \left(\Phi^{II}_{aug}\right)\left(u^1\right) \\ \left(\Phi^{II}_{aug}\right)\left(u^2\right) \\ \left(\Phi^{II}_{aug}\right)\left(u^3\right) \end{bmatrix} \qquad \text{with} \qquad \left(\Phi^{II}_{aug}\right)\left(u^j\right) = -u_j \tag{76}$$

The corresponding augmented constraint Jacobian in a decomposed fashion (67) is given by

$$\boldsymbol{G}^{II}_{aug}(\boldsymbol{u}) = \begin{bmatrix} -1 & 0 & 0 \\ 0 & -1 & 0 \\ 0 & 0 & -1 \end{bmatrix} = -\boldsymbol{I}_3 \tag{77}$$

For the sake of simplicity $\mathbf{G}^{I}_{aug}(q)$ will not be treated detailed, because its structure has already been presented in 4.2, (46).
The discrete counterpart of the equation above equals the expression itself.

5.3 Numerical example

As mentioned before our intention is to let body number 7 move upon a prescribed trajectory and calculate the necessary driving torques (input values) acting in the revolute joints. The desired trajectory shall follow a figure-8 pattern as similarly proposed in [MR06]:

$$\boldsymbol{\Phi}_{traj}(\boldsymbol{q}) = \begin{bmatrix} q^7_x(t_0) + \frac{1}{12}\sin(\omega(t)) \\ q^7_y(t_0) + \frac{1}{16}\sin(2\omega(t)) \end{bmatrix} \tag{78}$$

while **ω**(t) describes the angular velocity which for this example is defined as a 9th order polynomial. The polynomial was proposed in [BK04] and is well suited for control problems due to its continuous and steady character. In this example it is defined as followed:

$$\theta(t) = \begin{cases} s_1(t) & \text{for} \quad 0 \le t \le t_1 \\ s_2(t) & \text{for} \quad t_1 \le t \le t_2 \\ s_3(t) & \text{for} \quad t_2 \le t \le t_3 \end{cases} \tag{79}$$

where

$$\begin{aligned} s_1(t) &= \left[\tfrac{126}{6} t_1 \left(\tfrac{t}{t_1}\right)^6 - \tfrac{420}{7} t_1 \left(\tfrac{t}{t_1}\right)^7 + \tfrac{540}{8} t_1 \left(\tfrac{t}{t_1}\right)^8 - \tfrac{315}{9} t_1 \left(\tfrac{t}{t_1}\right)^9 + \tfrac{70}{10} t_1 \left(\tfrac{t}{t_1}\right)^{10} \right] \cdot \omega_0 \\ s_2(t) &= s_1(t_1) + \omega_0 (t - t_1) \\ s_3(t) &= s_2(t) - (t_3 - t_2) \cdot \left[\tfrac{126}{6} \left(\tfrac{t-t_2}{t_3-t_2}\right)^6 - \tfrac{420}{7} \left(\tfrac{t-t_2}{t_3-t_2}\right)^7 + \tfrac{540}{8} \left(\tfrac{t-t_2}{t_3-t_2}\right)^8 \right. \\ &\quad \left. - \tfrac{315}{9} \left(\tfrac{t-t_2}{t_3-t_2}\right)^9 + \tfrac{70}{10} \left(\tfrac{t-t_2}{t_3-t_2}\right)^{10} \right] \cdot \omega_0 \end{aligned} \tag{80}$$

Specifically we choose here

$$t_1 = 1s, \quad t_2 = 2s, \quad t_3 = 3s \quad \text{and} \quad \omega_0 = \pi \tag{81}$$

Since during this motion the inner triangle (body 7) shall not rotate we also have to implement another constraint suppressing the rotation

$$\boldsymbol{\Phi}^3(\boldsymbol{q}) = \boldsymbol{e}_2 \cdot \boldsymbol{d}_1^7 \tag{82}$$

The whole control constraint for the desired motion can then be written as:

$$\boldsymbol{\Phi}_C(\boldsymbol{q}) = \begin{bmatrix} \boldsymbol{\Phi}_{traj}(\boldsymbol{q}) \\ \boldsymbol{\Phi}^3(\boldsymbol{q}_0) \end{bmatrix} \tag{83}$$

The corresponding constraint Jacobian for the new control constraints yields:

$$\boldsymbol{B} = \begin{bmatrix} \boldsymbol{0}_{3\times 48} & \boldsymbol{I}_{3\times 3} & \boldsymbol{0}_{3\times 3} \end{bmatrix} \tag{84}$$

Since no external forces act on the system, its center of mass does not have to move. Moreover, since no external torques act on the system, the total angular momentum shall be a conserved quantity. The necessary driving torques to perform the desired motion are computed directly.

body	M	E_1	E_2	length	width
1	3	0.0125	0.0275	0.25	0.05
2	3	0.0125	0.0275	0.25	0.05
3	3	0.0125	0.0275	0.25	0.05
4	4	0.04	0.08	0.35	0.05
5	4	0.04	0.08	0.35	0.05
6	4	0.04	0.08	0.35	0.05

Table 3: Inertial and geometric properties pertaining to the six legs of the manipulator.

body	M	E_1	E_2	L
7	3	0.0408	0.0408	0.4
8	8	0.1	0.1	1.0

Table 4: Inertial and geometric properties pertaining to the two platforms of the manipulator.

Inertial and geometric properties of the rigid bodies constituting the parallel manipulator are summarized in Tables 3 and 4. In this connection, the two platforms (bodies 7 and 8) coincide with isosceles triangles of side-length L (Table 4).

The initial configuration of the closed-loop system can completely be specified by its generalized coordinates, accordingly

$$\boldsymbol{u}_0 = \begin{bmatrix} \boldsymbol{\varphi}^8(0)\cdot\boldsymbol{e}_1 \\ \boldsymbol{\varphi}^8(0)\cdot\boldsymbol{e}_2 \\ \theta^8(0) \\ \Theta^1(0) \\ \Theta^2(0) \\ \Theta^3(0) \\ \Theta^4(0) \\ \Theta^5(0) \\ \Theta^6(0) \\ \Theta^7(0) \end{bmatrix} = \begin{bmatrix} 0 \\ 0.2887 \\ 0 \\ \frac{\pi}{6} \\ \frac{2}{3}\pi \\ -\frac{\pi}{2} \\ \frac{\pi}{6} \\ \frac{2}{3}\pi \\ -\frac{\pi}{2} \\ 0 \end{bmatrix} \tag{85}$$

where the value of the initial posture of the small triangle (body 7) has been rounded for simplicity of exposition. As expected, the present energy-momentum schemes does indeed satisfy the above-mentioned conservation properties for any time step Δt, see Fig. 14. The simulated motion of the manipulator is illustrated in Fig. 16 by showing snapshots of the multibody system at subsequent points of time. The conservation of the total angular momentum also indicates that the position of the center of mass does not move for all times. The red glowing path in Fig. 16 corresponds to the trajectory of the center of mass of the small platform (body 7), representing the prescribed trajectory. Moreover, the evolution of the joint-angles $\Theta^1(t)$, $\Theta^2(t)$ and $\Theta^3(t)$, the translational displacements of the prismatic pairs $u_1(t)$, $u_2(t)$ and $u_3(t)$ calculated with a time step of $\Delta t = 0.02$, are depicted in Fig. 15 and Fig. 17. The necessary driving torques to perform the prescribed motion are displayed in Fig. 18.

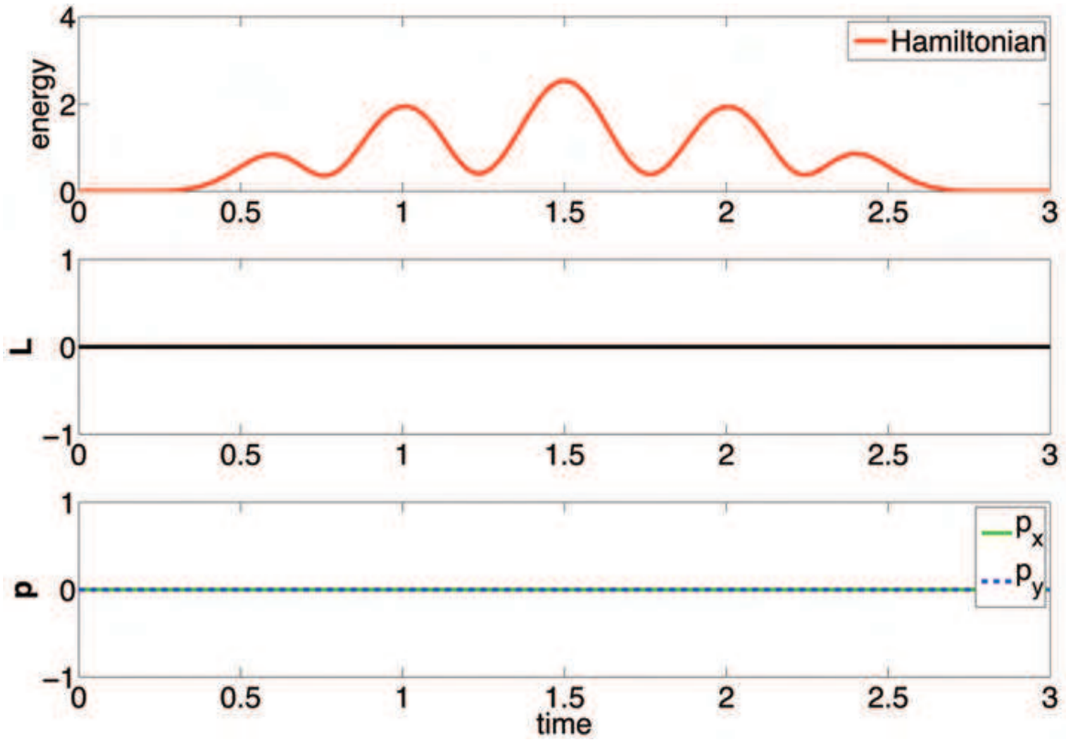

Figure 14: Total energy, conservation of angular and linear momentum ($\Delta t = 0.02$).

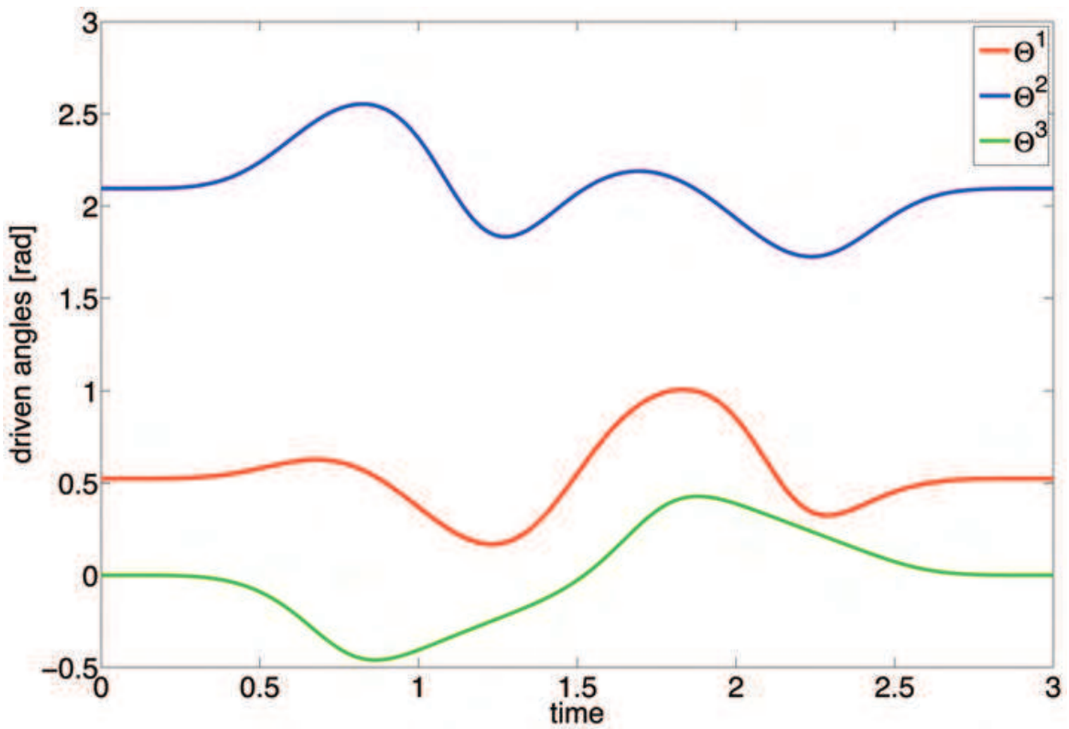

Figure 15: Joint-angles over time ($\Delta t = 0.02$).

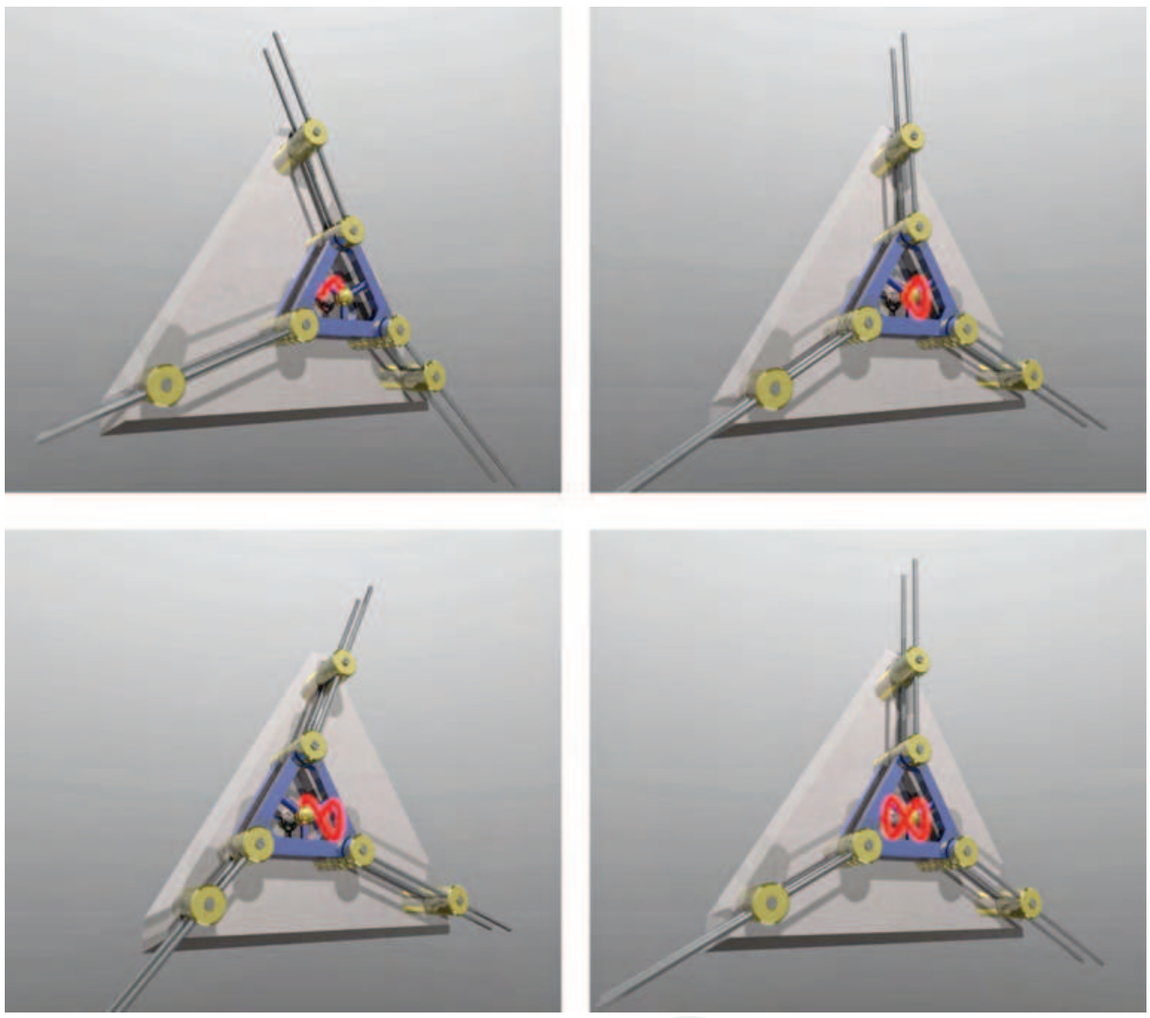

Figure 16: Snapshots of the motion of the free floating parallel manipulator for $t \in \{1, 1.5, 2, 3\}$s.

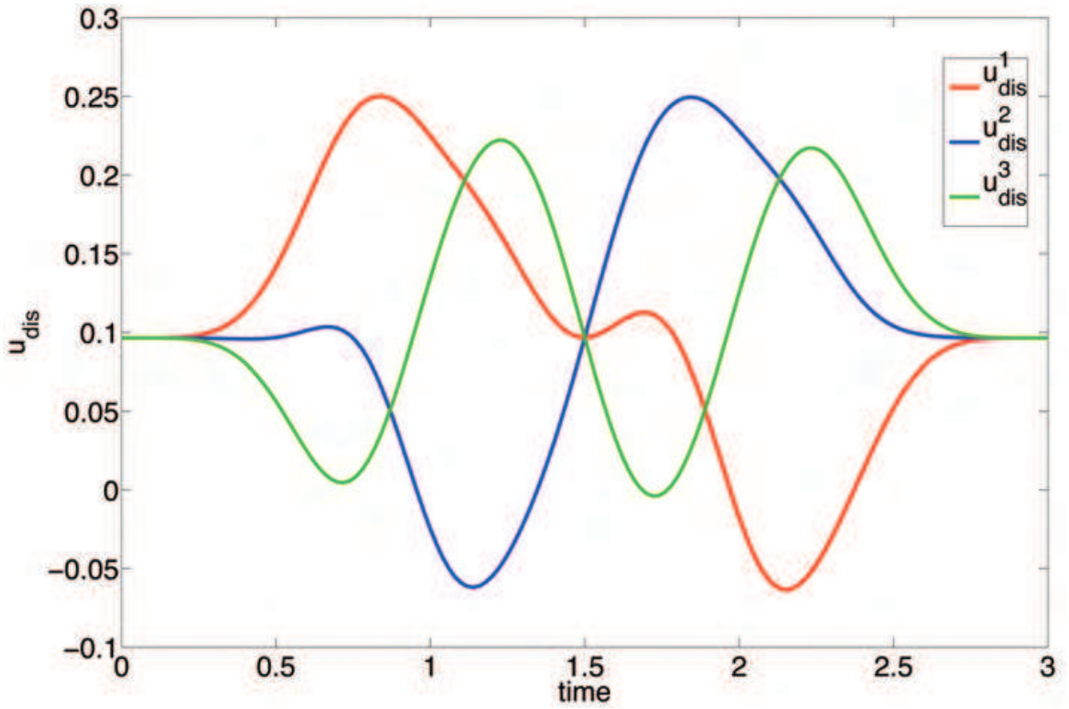

Figure 17: Augmented translational displacement over time (Δ t = 0.02).

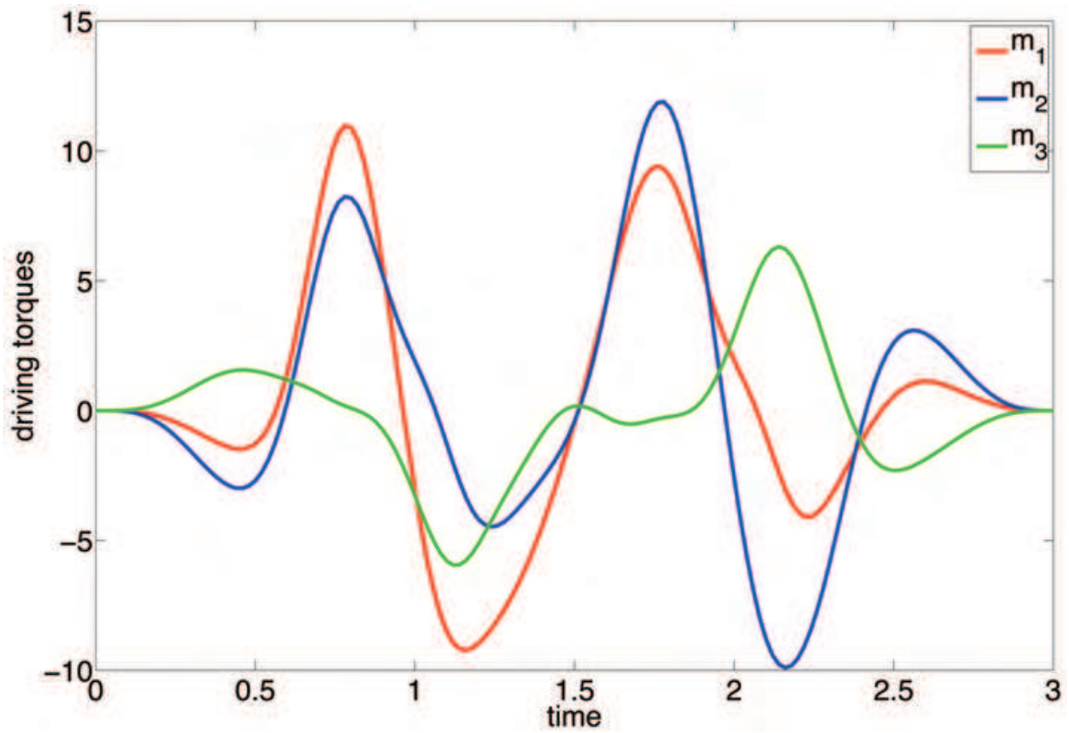

Figure 18: Driven joint-torques over time (Δ t = 0.02).

6. Conclusions

We have shown that the proposed rotationless formulation of multibody dynamics is well-suited for the energymomentum conserving integration of both open-loop and closed-loop multibody systems. Although the use of rotations has been completely circumvented throughout the whole discretization, joint-forces can still be applied to a specific multibody system by resorting to the proposed coordinate augmentation technique.

The present developments have been restricted to the planar case. However, it is important to note, that the extension to the three-dimensional setting can be performed without any conceptual differences. Similarly, alternative types of joints belonging to the class of lower kinematic pairs such as cylindric joints can be easily incorporated into the present approach. Both aforementioned issues have been addressed in [BL06].

The numerical examples presented herein have been specifically designed to check the algorithmic conservation properties. Within computational accuracy, the present approach facilitates the algorithmic conservation of energy as well as linear and angular momentum. Energy-momentum preserving schemes meet the specific demands on the stable numerical integration of the underlying index-3 DAEs. While the BEM scheme employed herein (cf. Section 2.1.1) is second-order accurate in the state space coordinates, higher-order energy-momentum schemes may be designed as set forth in [BS02a,GBS05]. The ostensible disadvantage of using redundant coordinates can be remedied by applying the size reduction techniques proposed in [BU07,BL06]. Specifically, it is shown in [BU07] that these techniques can be systematically applied to closed loop systems. Accordingly, they can be directly used in the example of the parallel manipulator dealt with in Section 5.

We have also presented the incorporation of servo / control constraints into our BEM scheme. This makes possible to perform a direct discretization for fully or underactuated systems and computing directly the necessary input values in order to control a system, without solving the standard inverse dynamics problem. Similar work has also been published in [BUQ].

It is further worth mentioning that semi-discrete formulations of flexible bodies such as nonlinear continua, beams and shells perfectly fit into the present framework provided by the DAEs (1). Accordingly, the present approach can be directly extended to flexible multibody dynamics (see [Bet06,Bet05b,LBS,SB]).

7. References

Armero, F.: Energy-dissipative momentum-conserving time-stepping algorithms for finite strain multiplicative plasticity. In: *Comput. Methods Appl. Mech. Engrg.* 195 (2006), S. 4862–4889

Bauchau, O.A. ; Bottasso, C.L.: On the design of energy preserving and decaying schemes for flexible, nonlinear multi-body systems. In: *Comput. Methods Appl. Mech. Engrg.* 169 (1999), S. 61–79

Brank, B. ; Briseghella, L. ; Tonello, N. ; Damjanic, F.B.: On Non-Linear Dynamics of Shells: Implementation of Energy-Momentum Conserving Algorithm for a Finite Rotation Shell Model. In: *Int. J. Numer. Methods Eng.* 42 (1998), S. 409–442

Betsch, P.: The discrete null space method for the energy consistent integration of constrained mechanical systems. Part I: Holonomic constraints. In: *Comput. Methods Appl. Mech. Engrg.* 194 (2005), Nr. 50-52, S. 5159–5190

Betsch, P.: On the discretization of geometrically exact shells for flexible multibody dynamics. In: *Proceedings of the ECCOMAS Thematic Conference on Multibody Dynamics (on CD)*. Madrid, Spain, 21-24 June 2005, S. 1–13

Betsch, P.: Energy-consistent numerical integration of mechanical systems with mixed holonomic and nonholonomic constraints. In: *Comput. Methods Appl. Mech. Engrg.* 195 (2006), S. 7020–7035

Blajer, W. ; Ko!lodziejczyk, K.: A Geometric Approach to Solving Problems of Control Constraints: Theory and a DAE Framework. In: *Multibody System Dynamics* 11 (2004), Nr. 4, S. 343–364

Betsch, P. ; Leyendecker, S.: The discrete null space method for the energy consistent integration of constrained mechanical systems. Part II: Multibody dynamics. In: *Int. J. Numer. Methods Eng.* 67 (2006), Nr. 4, S. 499–552

Betsch, P. ; Steinmann, P.: Conservation Properties of a Time FE Method. Part II: Time-Stepping Schemes for Nonlinear Elastodynamics. In: *Int. J. Numer. Methods Eng.* 50 (2001), S. 1931–1955

Betsch, P. ; Steinmann, P.: Constrained Integration of Rigid Body Dynamics. In: *Comput.Methods Appl. Mech. Engrg.* 191 (2001), S. 467–488

Betsch, P. ; Steinmann, P.: Conservation Properties of a Time FE Method. Part III: Mechanical systems with holonomic constraints. In: *Int. J. Numer. Methods Eng.* 53 (2002), S. 2271–2304

Betsch, P. ; Steinmann, P.: A DAE approach to flexible multibody dynamics. In: *Multibody System Dynamics* 8 (2002), S. 367–391

Betsch, P. ; Uhlar, S.: Energy-momentum conserving integration of multibody dynamics. In: *Multibody System Dynamics* 17 (2007), Nr. 4, S. 243–289

Betsch, P. ; Uhlar, S. ; Quasem, M.: *On the incorporation of servo constraints into a rotationless formulation of flexible multibody dynamics*. In Proceedings of the ECCOMAS Thematic Conference on Multibody Dynamics, 25-28 June 2007, Milano, Italy,

Crisfield, M.A. ; Jeleni´c, G.: Energy/Momentum Conserving Time Integration Procedures with Finite Elements and Large Rotations. In: Ambr´osio, J. (Hrsg.) ; Kleiber, M. (Hrsg.): *NATOARW on Comp. Aspects of Nonlin. Struct. Sys. with Large Rigid Body Motion*. Pultusk, Poland, July 2-7, 2000, S. 181–200

Groß, M. ; Betsch, P. ; Steinmann, P.: Conservation properties of a time FE method. Part IV: Higher order energy and momentum conserving schemes. In: *Int. J. Numer. Methods Eng.* 63 (2005), S. 1849–1897

G´eradin, M. ; Cardona, A.: *Flexible multibody dynamics: A finite element approach*. John Wiley & Sons, 2001

Goicolea, J.M. ; Garcia Orden, J.C.: Dynamic analysis of rigid and deformable multibody systems with penalty methods and energy-momentum schemes. In: *Comput. Methods Appl. Mech. Engrg.* 188 (2000), S. 789–804

Gonzalez, O.: Time Integration and Discrete Hamiltonian Systems. In: *J. Nonlinear Sci.* 6 (1996), S. 449–467

Gonzalez, O.: Mechanical Systems Subject to Holonomic Constraints: Differential-Algebraic Formulations and Conservative Integration. In: *Physica D* 132 (1999), S. 165–174

Greenspan, D.: Conservative Numerical Methods for $\ddot{x} = f(x)$. In: *Journal of Computational Physics* 56 (1984), S. 28–41

Gonzalez, O. ; Simo, J.C.: On the Stability of Symplectic and Energy-Momentum Algorithms for non-linear Hamiltonian Systems with Symmetry. In: *Comput. Methods Appl. Mech. Engrg.* 134 (1996), S. 197–222

Ibrahimbegovi´c, A. ; Mamouri, S. ; Taylor, R.L. ; Chen, A.J.: Finite Element Method in Dynamics of Flexible Multibody Systems: Modeling of Holonomic Constraints and Energy Conserving Integration Schemes. In: *Multibody System Dynamics* 4 (2000), Nr. 2-3, S. 195–223

Jalon, J. Garcia d. ; Unda, J. ; Avello, A.: Natural coordinates for the computer analysis of multibody systems. In: *Comput. Methods Appl. Mech. Engrg.* 56 (1986), S. 309–327

Kunkel, P. ; Mehrmann, V.: *Differential-Algebraic Equations*. European Mathematical Society,2006

Leyendecker, S. ; Betsch, P. ; Steinmann, P.: *The discrete null space method for the energy consistent integration of constrained mechanical systems. Part III: Flexible multibody dynamics*. Accepted for publication in Multibody System Dynamics,

Leyendecker, S. ; Betsch, P. ; Steinmann, P.: Energy-conserving integration of constrained Hamiltonian systems - a comparison of approaches. In: *Computational Mechanics* 33 (2004), Nr. 3, S. 174–185

Laursen, T.A. ; Love, G.R.: Improved implicit integrators for transient impact problems–geometric admissibility withing the conserving framework. In: *Int. J. Numer. Methods Eng.* 53 (2002), S. 245–274

Leimkuhler, B. ; Reich, S.: *Simulating Hamiltonian Dynamics*. Cambridge University Press, 2004

McPhee, J.J. ; Redmond, S.M.: Modelling multibody systems with indirect coordinates. In: *Comput. Methods Appl. Mech. Engrg.* 195 (2006), S. 6942–6957

Puso, M.A.: An energy and momentum conserving method for rigid-flexible body dynamics. In: *Int. J. Numer. Methods Eng.* 53 (2002), S. 1393–1414

Romero, I. ; Armero, F.: An objective finite element approximation of the kinematics of geometrically exact rods and its use in the formulation of an energy-momentum conserving scheme in dynamics. In: *Int. J. Numer. Methods Eng.* 54 (2002), S. 1683–1716

Rosenberg, R.M.: *Analytical dynamics of discrete systems*. Plenum Press, 1977

Rubin, H. ; Ungar, P.: Motion under a strong constraining force. In: *Commun. Pure Appl. Math.* 10 (1957), Nr. 1, S. 65–87

S¨anger, N. ; Betsch, P.: *A uniform rotationless formulation of flexible multibody dynamics: Conserving integration of rigid bodies, nonlinear beams and shells*. In Proceedings of the ECCOMAS Thematic Conference on Multibody Dynamics, 25 28 June 2007, Milano, Italy,

Simo, J.C. ; Tarnow, N.: The Discrete Energy-Momentum Method. Conserving Algorithms for Nonlinear Elastodynamics. In: *Z. angew. Math. Phys. (ZAMP)* 43 (1992), S. 757–792

Simo, J.C. ; Tarnow, N. ; Wong, K.K.: Exact Energy-Momentum Conserving Algorithms and Symplectic Schemes for Nonlinear Dynamics. In: *Comput. Methods Appl. Mech. Engrg.* 100 (1992), S. 63–116

Simo, J.C. ; Wong, K.K.: Unconditionally Stable Algorithms for Rigid Body Dynamics that Exactly Preserve Energy and Momentum. In: *Int. J. Numer. Methods Eng.* 31 (1991), S. 19–52

Parallel Manipulators, New Developments

Edited by Jee-Hwan Ryu

ISBN 978-3-902613-20-2

Hard cover, 498 pages

Publisher I-Tech Education and Publishing

Published online 01, April, 2008

Published in print edition April, 2008

Parallel manipulators are characterized as having closed-loop kinematic chains. Compared to serial manipulators, which have open-ended structure, parallel manipulators have many advantages in terms of accuracy, rigidity and ability to manipulate heavy loads. Therefore, they have been getting many attentions in astronomy to flight simulators and especially in machine-tool industries.The aim of this book is to provide an overview of the state-of-art, to present new ideas, original results and practical experiences in parallel manipulators. This book mainly introduces advanced kinematic and dynamic analysis methods and cutting edge control technologies for parallel manipulators. Even though this book only contains several samples of research activities on parallel manipulators, I believe this book can give an idea to the reader about what has been done in the field recently, and what kind of open problems are in this area.

InTech Europe

University Campus STeP Ri
Slavka Krautzeka 83/A
51000 Rijeka, Croatia
Phone: +385 (51) 770 447
Fax: +385 (51) 686 166
www.intechopen.com

InTech China

Unit 405, Office Block, Hotel Equatorial Shanghai
No.65, Yan An Road (West), Shanghai, 200040, China
中国上海市延安西路65号上海国际贵都大饭店办公楼405单元
Phone: +86-21-62489820
Fax: +86-21-62489821

IntechOpen